The benefits of $\bar{B} \to \bar{K}^* l^+ l^-$ decays at low recoil

Christoph Bobeth,[a] **Gudrun Hiller**[b,c] **and Danny van Dyk**[c]

[a] *IPHC, Université de Strasbourg,*
CNRS/IN2P3, F-67037, Strasbourg, France

[b] *CERN, Theory Division,*
CH-1211 Geneva 23, Switzerland

[c] *Institut für Physik, Technische Universität Dortmund,*
D-44221 Dortmund, Germany

E-mail: bobeth@ires.in2p3.fr, gudrun.hiller@udo.edu, danny.dyk@udo.edu

ABSTRACT: Using the heavy quark effective theory framework put forward by Grinstein and Pirjol we work out predictions for $\bar{B} \to \bar{K}^* l^+ l^-$, $l = e, \mu$, decays for a softly recoiling $\bar{K}^*$, i.e., for large dilepton masses $\sqrt{q^2}$ of the order of the b-quark mass m_b. We work to lowest order in Λ/Q, where $Q = (m_b, \sqrt{q^2})$ and include the next-to-leading order corrections from the charm quark mass m_c and the strong coupling at $\mathcal{O}(m_c^2/Q^2, \alpha_s)$. The leading Λ/m_b corrections are parametrically suppressed. The improved Isgur-Wise form factor relations correlate the $\bar{B} \to \bar{K}^* l^+ l^-$ transversity amplitudes, which simplifies the description of the various decay observables and provides opportunities for the extraction of the electroweak short distance couplings. We propose new angular observables which have very small hadronic uncertainties. We exploit existing data on $\bar{B} \to \bar{K}^* l^+ l^-$ distributions and show that the low recoil region provides powerful additional information to the large recoil one. We find disjoint best-fit solutions, which include the Standard Model, but also beyond-the-Standard Model ones. This ambiguity can be accessed with future precision measurements.

KEYWORDS: Rare Decays, B-Physics, Beyond Standard Model

ArXiv ePrint: 1006.5013

Contents

1 Introduction

The study of b-flavored mesons made possible our current understanding of quark flavor violation in the Standard Model (SM) [1, 2]. It is an ongoing endeavour to map out the flavor sector at the electroweak scale and beyond, and possibly thereby gaining insights on the origin of flavor.

In this effort, flavor changing neutral current-induced exclusive B decays into dileptons are important modes because of their sensitivity to physics beyond the SM and their accessibility at current collider experiments and possible future high luminosity facilities [3–6].

We focus in this work on the semileptonic decays $\bar{B} \to \bar{K}^* l^+ l^-$ with $l = e, \mu$. Their branching ratios are measured at $\mathcal{O}(10^{-7} - 10^{-6})$ [7], consistent with the SM [8]. Beyond the rate, several observables can be obtained from the rare decays, in particular when analyzed through $\bar{B} \to \bar{K}^* (\to \bar{K}\pi) l^+ l^-$ [9]. The presence of multiple observables is advantageous because they are, in general, complementary in their sensitivity to the electroweak

couplings, and they provide opportunities to control uncertainties. This is even more important nowadays, as flavor physics data are favoring the amount of fundamental flavor violation being at least not far away from the one in the SM, and require a certain level of precision to be observed.

Recently, data have become available on $\bar{B} \to \bar{K}^* l^+ l^-$ decay distributions in the dilepton invariant mass, $\sqrt{q^2}$, from the experiments BaBar [10, 11], Belle [12] and CDF [13]. These experimental studies cover essentially the full kinematical dilepton mass range, with the exception of the regions around $q^2 \sim m_{J/\psi}^2$ and $q^2 \sim m_{\psi'}^2$. Here, cuts are employed to remove the overwhelming background induced by $\bar{B} \to \bar{K}^*(\bar{c}c) \to \bar{K}^* l^+ l^-$ from the dominant charmonium resonances $(\bar{c}c) = J/\psi, \psi'$.

Most theoretical works on $\bar{B} \to \bar{K}^* l^+ l^-$ decays over the past years have focussed on the region of large recoil, that is, small $q^2 \lesssim m_{J/\psi}^2$. However, at low recoil (large $q^2 \gtrsim m_{\psi'}^2$) dedicated studies are lacking with a similar QCD-footing as the ones at large recoil, where QCD factorization (QCDF) applies [14, 15]. It is the goal of this work to fill this gap and benefit from the incoming and future physics data from the low recoil region as well.

We use the heavy quark effective theory (HQET) framework by Grinstein and Pirjol [16], which is applicable to the low recoil region, where $\sqrt{q^2}$ is of the order of the mass of the b-quark, m_b, and the emitted vector meson is soft in the B mesons rest frame. The original application was to extract the Cabibbo Kobayashi Maskawa (CKM) matrix element V_{ub} by relating the dilepton spectra of $\bar{B} \to \rho l \nu$ to those in $\bar{B} \to \bar{K}^* l^+ l^-$ decays. The framework has also been used previously to study the implications of the sign of the forward-backward asymmetry in $\bar{B} \to \bar{K}^* l^+ l^-$ decays being determined SM-like for large q^2 [17], see also [18] for relating $\bar{B} \to \bar{K} l^+ l^-$ to $\bar{B} \to \bar{K} \nu \bar{\nu}$ decays. Here, we work out and analyze in detail distributions of $\bar{B} \to \bar{K}^* l^+ l^-$ decays in this low recoil framework and give predictions within the SM and beyond.

The description of $\bar{B} \to \bar{K}^* l^+ l^-$ decays at low recoil is based on two ingredients: the improved Isgur-Wise form factor relations [16, 19], going beyond the original ones [20], and an operator product expansion (OPE) in $1/Q$, where $Q = (m_b, \sqrt{q^2})$ [16]. The latter allows to include the contributions from quark loops, most notably charm loops in a model-independent way. Both ingredients are first principle effective field theory tools and allow to obtain the $\bar{B} \to \bar{K}^* l^+ l^-$ matrix element in a systematic expansion in the strong coupling and in power corrections suppressed by the heavy quark mass. The implementation of continuum and resonance $\bar{c}c$ effects from $e^+ e^- \to hadrons$ data [21] suggests no large duality violation at least above the ψ', supporting the aforementioned OPE.

We work to lowest order in Λ/m_b, however, the actual leading power corrections to the decay amplitudes arise only at order $\alpha_s \Lambda/m_b$ or with other parametric suppression factors, and amount only to a few percent.

The plan of the paper is as follows: In section 2 we give the electroweak Hamiltonian responsible for $b \to s l^+ l^-$ processes and review the observables in $\bar{B} \to \bar{K}^* l^+ l^-$ decays. The low recoil framework is summarized in section 3, where the $\bar{B} \to \bar{K}^* l^+ l^-$ transversity amplitudes and observables are computed and correlations are pointed out. SM predictions and the comparison with the data are given in section 4. We conclude in section 5. In several appendices we give formulae and detailed input for our analysis.

2 Generalities

We define the short distance couplings entering $b \to sl^+l^-$ decays in section 2.1 and introduce in section 2.2 the observables in $\bar{B} \to \bar{K}^*l^+l^-$ decays, where the former can be tested.

2.1 Quark level

For the description of processes induced by $b \to sl^+l^-$ we use an effective $\Delta B = 1$ electroweak Hamiltonian

$$\mathcal{H}_{\text{eff}} = -\frac{4G_{\text{F}}}{\sqrt{2}} V_{tb}V_{ts}^* \sum_i \mathcal{C}_i(\mu)\mathcal{O}_i(\mu) + \text{h.c.,} \tag{2.1}$$

which consists of the higher dimensional operators $\mathcal{O}_i$ and their respective Wilson coefficients $\mathcal{C}_i$. Here, μ denotes the renormalization scale, G_{F} is Fermi's constant and $V_{tb}V_{ts}^*$ collects the leading flavor factors of the SM encoded in the CKM matrix elements V_{ij}. We neglect subleading contributions of the order $V_{ub}V_{us}^*$, hence, there is no CP violation in the SM in the decay amplitudes. We also set the strange quark mass to zero.

For the decays $b \to sl^+l^-$ the electromagnetic dipole ($\mathcal{O}_7$) and semileptonic four-fermion ($\mathcal{O}_{9,10}$) operators are the most relevant:

$$\mathcal{O}_7 = \frac{e}{(4\pi)^2} m_b \left[\bar{s}\sigma^{\mu\nu}P_R b\right] F_{\mu\nu}, \qquad \mathcal{O}_8 = \frac{g_s}{(4\pi)^2} m_b \left[\bar{s}\sigma^{\mu\nu}P_R T^a b\right] G^a_{\mu\nu},$$

$$\mathcal{O}_9 = \frac{e^2}{(4\pi)^2} \left[\bar{s}\gamma_\mu P_L b\right] \left[\bar{l}\gamma^\mu l\right], \qquad \mathcal{O}_{10} = \frac{e^2}{(4\pi)^2} \left[\bar{s}\gamma_\mu P_L b\right] \left[\bar{l}\gamma^\mu \gamma_5 l\right], \tag{2.2}$$

where $P_{L,R}$ denote chiral projectors, m_b is the $\overline{\text{MS}}$ mass of the b-quark and $F_{\mu\nu}(G^a_{\mu\nu})$ is the field strength tensor of the photon (gluons $a = 1, \ldots, 8$). The contributions from the gluonic dipole operator $\mathcal{O}_8$ enter the semileptonic decay amplitude at higher order in the strong coupling g_s, and have a significantly reduced sensitivity to New Physics as compared to those from $\mathcal{O}_{7,9,10}$. For the current-current and QCD-penguin operators $\mathcal{O}_{1\ldots6}$ we use the definitions of ref. [22]. We call the set of operators eq. (2.2) plus the four-quark operators $\mathcal{O}_{1\ldots6}$ the SM basis, and stay in this work within this basis.

The goal of this work is to extract from b-physics data the coefficients $\mathcal{C}_{7,9,10}$ and test them against their respective SM predictions. All other Wilson coefficients are fixed to their respective SM values. We restrict ourselves to real-valued Wilson coefficients, hence allow for no CP violation beyond the SM. We made this choice because existing CP data on the $b \to sl^+l^-$ transitions [7], which are consistent with our assumption, are currently quite limited, have rather large uncertainties, and the inclusion of phases doubles the number of parameters in the fit. We hope to come back to this in the future.

In the following we understand all Wilson coefficients being evaluated at the scale of the b-quark mass. In the SM at next-to-leading order their values are approximately, for $\mu = m_b$,

$$\mathcal{C}_7^{\text{SM}} = -0.3, \qquad \mathcal{C}_9^{\text{SM}} = 4.2, \qquad \mathcal{C}_{10}^{\text{SM}} = -4.2. \tag{2.3}$$

The coefficient of $\mathcal{O}_7$ is suppressed with respect to the ones of $\mathcal{O}_{9,10}$, a feature that holds in many extensions of the SM as well, and is also respected by the data. This hierarchy in coupling strengths is beneficial for controlling theoretical uncertainties, see section 3.

We neglect lepton flavor non-universal effects, hence, the couplings to $l = e$ and $l = \mu$ are considered to be equal. For recent works exploiting the possibility that New Physics affects the final state electron and muon pairs differently, see, *e.g.,* [23]. Since the decays $b \to s\tau^+\tau^-$ are experimentally difficult and have not been seen so far, we do not consider taus and can neglect the lepton masses.

2.2 The $\bar{B} \to \bar{K}^* l^+ l^-$ observables

Angular analysis offers the maximal information which is accessible from the decay via $\bar{B} \to \bar{K}^*(\to \bar{K}\pi)l^+l^-$. For an on-shell $\bar{K}^*$ the differential decay width can be written as [9, 24]

$$\frac{\mathrm{d}^4\Gamma}{\mathrm{d}q^2 \mathrm{d}\cos\theta_l \mathrm{d}\cos\theta_{K^*}\mathrm{d}\phi} = \frac{3}{8\pi}J(q^2, \cos\theta_l, \cos\theta_{K^*}, \phi), \tag{2.4}$$

where the lepton spins have been summed over. Here, q^2 is the dilepton invariant mass squared, that is, q^μ is the sum of $p_{l^+}^\mu$ and $p_{l^-}^\mu$, the four momenta of the positively and negatively charged lepton, respectively. Furthermore, θ_l is defined as the angle between the negatively charged lepton and the $\bar{B}$ in the dilepton center of mass system (c.m.s.) and θ_{K^*} is the angle between the Kaon and the $\bar{B}$ in the $(K^-\pi^+)$ c.m.s.. We denote by $\mathbf{p}_i$ the three momentum vector of particle i in the $\bar{B}$ rest frame. Then, ϕ is given by the angle between $\mathbf{p}_{K^-} \times \mathbf{p}_{\pi^+}$ and $\mathbf{p}_{l^-} \times \mathbf{p}_{l^+}$, i.e., the angle between the normals of the $(K^-\pi^+)$ and (l^-l^+) planes.

The full kinematically accessible phase space is bounded by

$$4m_l^2 \leqslant q^2 \leqslant (m_B - m_{K^*})^2, \quad -1 \leqslant \cos\theta_l \leqslant 1, \quad -1 \leqslant \cos\theta_{K^*} \leqslant 1, \quad 0 \leqslant \phi \leqslant 2\pi, \tag{2.5}$$

where m_l, m_B and m_{K^*} denote the mass of the lepton, B meson and the K^*, respectively.

The dependence of the decay distribution eq. (2.4) on the angles θ_l, θ_{K^*} and ϕ can be made explicit as

$$\begin{aligned}
J(q^2, \theta_l, \theta_{K^*}, \phi) = {} & J_1^s \sin^2\theta_{K^*} + J_1^c \cos^2\theta_{K^*} + (J_2^s \sin^2\theta_{K^*} + J_2^c \cos^2\theta_{K^*})\cos 2\theta_l \\
& + J_3 \sin^2\theta_{K^*}\sin^2\theta_l \cos 2\phi + J_4 \sin 2\theta_{K^*}\sin 2\theta_l \cos\phi \\
& + J_5 \sin 2\theta_{K^*}\sin\theta_l \cos\phi + J_6 \sin^2\theta_{K^*}\cos\theta_l + J_7 \sin 2\theta_{K^*}\sin\theta_l \sin\phi \\
& + J_8 \sin 2\theta_{K^*}\sin 2\theta_l \sin\phi + J_9 \sin^2\theta_{K^*}\sin^2\theta_l \sin 2\phi, \tag{2.6}
\end{aligned}$$

where the angular coefficients $J_i^{(a)} = J_i^{(a)}(q^2)$ for $i = 1, \ldots, 9$ and $a = s, c$ are functions of the dilepton mass. We suppress in the following the q^2-dependence also in expressions derived from the $J_i^{(a)}$. The latter can be written in terms of the transversity amplitudes $A_{\perp,\parallel,0}$, see appendix A. The fourth amplitude A_t does not contribute in the limit $m_l = 0$. The transversity amplitudes at low recoil are given in the next section. The ones at large recoil can be seen, for example, in ref. [17].

The angular coefficients $J_i^{(a)}$, or their normalized variants $J_i/(\mathrm{d}\Gamma/\mathrm{d}q^2)$ or J_i/J_j, are observables which can be extracted from an angular analysis. This method allows to test the SM and probe a multitude of different couplings [17, 24–27]. We focus first on rather simple observables, which can be extracted without performing a statistics intense full angular analysis. Afterwards, we point out opportunities of measuring the angular distribution.

Data on $\bar{B} \to \bar{K}^* l^+ l^-$ decays already exists from BaBar [10, 11], Belle [12] and CDF [13] for the differential decay width $\mathrm{d}\Gamma/\mathrm{d}q^2$, the forward-backward asymmetry A_{FB} and the fraction of longitudinal polarized K^*'s, F_{L}. They are written as

$$\frac{\mathrm{d}\Gamma}{\mathrm{d}q^2} = 2J_1^s + J_1^c - \frac{2J_2^s + J_2^c}{3} = |A_0^L|^2 + |A_\perp^L|^2 + |A_\parallel^L|^2 + (L \leftrightarrow R), \tag{2.7}$$

$$A_{\mathrm{FB}} = \left[\int_0^1 - \int_{-1}^0 \right] \mathrm{d}\cos\theta_l \, \frac{\mathrm{d}^2\Gamma}{\mathrm{d}q^2 \, \mathrm{d}\cos\theta_l} \bigg/ \frac{\mathrm{d}\Gamma}{\mathrm{d}q^2} = \frac{J_6}{\mathrm{d}\Gamma/\mathrm{d}q^2}, \tag{2.8}$$

$$F_{\mathrm{L}} = \frac{|A_0^L|^2 + |A_0^R|^2}{\mathrm{d}\Gamma/\mathrm{d}q^2}, \tag{2.9}$$

and are all distributions in the dilepton mass.

The experimental data on the q^2-distributions [10–13] are currently available in q^2-bins, i.e., the decay rate is given as a list of rates $\langle \mathrm{d}\Gamma/\mathrm{d}q^2 \rangle_k$, where we denote by $\langle \ldots \rangle_k$ the $\mathrm{d}q^2$-integration over the k-th bin. Normalized quantities such as the forward-backward asymmetry are then delivered as $\langle J_6 \rangle_k / \langle \mathrm{d}\Gamma/\mathrm{d}q^2 \rangle_k$, and likewise as $\langle |A_0^L|^2 + |A_0^R|^2 \rangle_k / \langle \mathrm{d}\Gamma/\mathrm{d}q^2 \rangle_k$ for the longitudinal polarization fraction. The binned distributions equal our definitions eqs. (2.8) and (2.9) for flat distributions or infinitely small bin size.

Note that the $J_{5,6,8,9}$, and hence A_{FB} are CP-odd observables, which vanish in an untagged equally mixed sample of $\bar{B}$ and B decays in the absence of CP violation [17].

We also consider the transverse asymmetries $A_T^{(2)}$ [24] and $A_T^{(3,4)}$ [25], given as

$$A_T^{(2)} = \frac{|A_\perp^L|^2 + |A_\perp^R|^2 - |A_\parallel^L|^2 - |A_\parallel^R|^2}{|A_\perp^L|^2 + |A_\perp^R|^2 + |A_\parallel^L|^2 + |A_\parallel^R|^2}$$
$$= \frac{1}{2} \frac{J_3}{J_2^s}, \tag{2.10}$$

$$A_T^{(3)} = \frac{|A_0^L A_\parallel^{L*} + A_0^{R*} A_\parallel^R|}{\sqrt{\left(|A_0^L|^2 + |A_0^R|^2\right)\left(|A_\perp^L|^2 + |A_\perp^R|^2\right)}}$$
$$= \sqrt{\frac{4J_4^2 + \beta_l^2 J_7^2}{-2J_2^c(2J_2^s + J_3)}}, \tag{2.11}$$

$$A_T^{(4)} = \frac{|A_0^L A_\perp^{L*} - A_0^{R*} A_\perp^R|}{|A_0^{L*} A_\parallel^L + A_0^R A_\parallel^{R*}|}$$
$$= \sqrt{\frac{\beta_l^2 J_5^2 + 4J_8^2}{4J_4^2 + \beta_l^2 J_7^2}}, \tag{2.12}$$

which have not been measured yet. The factor β_l is given in appendix A. Here we keep the lepton mass dependence for generality but discard it later on when discussing the low recoil region where m_l is entirely neglibile.

We propose the following new transversity observables for the region of low recoil (high q^2)

$$H_T^{(1)} = \frac{\text{Re}(A_0^L A_\parallel^{L*} + A_0^{R*} A_\parallel^R)}{\sqrt{\left(|A_0^L|^2 + |A_0^R|^2\right)\left(|A_\parallel^L|^2 + |A_\parallel^R|^2\right)}} = \frac{\sqrt{2} J_4}{\sqrt{-J_2^c\left(2J_2^s - J_3\right)}}, \qquad (2.13)$$

$$H_T^{(2)} = \frac{\text{Re}(A_0^L A_\perp^{L*} - A_0^{R*} A_\perp^R)}{\sqrt{\left(|A_0^L|^2 + |A_0^R|^2\right)\left(|A_\perp^L|^2 + |A_\perp^R|^2\right)}} = \frac{\beta_l J_5}{\sqrt{-2J_2^c\left(2J_2^s + J_3\right)}}, \qquad (2.14)$$

$$H_T^{(3)} = \frac{\text{Re}(A_\parallel^L A_\perp^{L*} - A_\parallel^{R*} A_\perp^R)}{\sqrt{\left(|A_\parallel^L|^2 + |A_\parallel^R|^2\right)\left(|A_\perp^L|^2 + |A_\perp^R|^2\right)}} = \frac{\beta_l J_6}{2\sqrt{(2J_2^s)^2 - J_3^2}}. \qquad (2.15)$$

As will become clear in section 3, see also appendix B, the $H_T^{(i)}$ are designed to have very small hadronic uncertainties at low recoil. While both $H_T^{(3)}$ and A_{FB} depend on J_6 and probe similar short distance physics, the former has a significantly smaller theoretical uncertainty than the latter. Note also that the numerator J_5 of $H_T^{(2)}$ is related to the observable S_5 which has good prospects to be measured with early LHCb data of $2\,\text{fb}^{-1}$ at least in the large recoil region [28].

Different possibilities to extract the J_i from single differential distributions as well have been outlined in [17].

3 $\bar{B} \to \bar{K}^* l^+ l^-$ at low recoil

We start in section 3.1 with the model-independent description of the exclusive heavy-to-light decays in the low recoil region following Grinstein and Pirjol [16, 19]. After calculating and investigating the $\bar{B} \to \bar{K}^* l^+ l^-$ transversity amplitudes in section 3.2, we work out predictions for and correlations between the $\bar{B} \to \bar{K}^* l^+ l^-$ observables at low recoil in section 3.3. A numerical study within the SM is given in section 4.1.

3.1 The model-independent framework

The description of $\bar{B} \to \bar{K}^* l^+ l^-$ decays at low recoil, where $q^2 \sim \mathcal{O}(m_b^2)$, is based on the improved form factor relations in this region and an OPE in $1/Q$ [16, 19]. The latter keeps the non-perturbative contributions from 4-quark operators $(\bar{s}b)(\bar{q}q)$ under control by expanding in m_q^2/Q^2. This is most important for charm quarks, since their operators can enter with no suppression from small Wilson coefficients nor CKM matrix elements.

Following [16] we briefly sketch the derivation of the improved Isgur-Wise form factor relations to leading order in $1/m_b$ between the vector and the tensor current. The starting point is the QCD operator identity (for $m_s = 0$)

$$i\partial^\nu(\bar{s}i\sigma_{\mu\nu}b) = -m_b\bar{s}\gamma_\mu b + i\partial_\mu(\bar{s}b) - 2\bar{s}i\overleftarrow{D}_\mu b. \qquad (3.1)$$

After taking the matrix element of eq. (3.1) using the form factors given in appendix C one arrives at an exact relation between the form factors T_1 and V and the matrix element

of the current $\bar{s}i\overleftarrow{D}_\mu b$. The latter can be expanded in $1/m_b$ through matching onto the HQET currents with the heavy quark field h_v:

$$\bar{s}i\overleftarrow{D}_\mu b = D_0^{(v)}(\mu)m_b\bar{s}\gamma_\mu h_v + D_1^{(v)}(\mu)m_b v_\mu \bar{s}h_v + \ldots. \tag{3.2}$$

We further need

$$\bar{s}\gamma_\mu b = C_0^{(v)}(\mu)\bar{s}\gamma_\mu h_v + C_1^{(v)}(\mu)v_\mu \bar{s}h_v + \ldots, \tag{3.3}$$

$$\bar{s}b = C_0^{(s)}(\mu)\bar{s}h_v + \ldots, \tag{3.4}$$

to express the HQET currents in eq. (3.2) through quark currents. The ellipses denote power suppressed contributions. The Wilson coefficients $C_i^{(x)}$ and $D_i^{(x)}$ are calculable and known in a perturbative expansion in the strong coupling, see, e.g., [16, 29].

Taking then the matrix element of eq. (3.2) yields

$$\langle K^*|\bar{s}i\overleftarrow{D}_\mu b|B\rangle = \frac{m_b D_0^{(v)}(\mu)}{C_0^{(v)}(\mu)}\langle K^*|\bar{s}\gamma_\mu b|B\rangle + \ldots. \tag{3.5}$$

After working out the corresponding formulae involving the axial currents, the improved Isgur-Wise relations to leading order in $1/m_b$ including radiative corrections are obtained as

$$T_1(q^2) = \kappa V(q^2), \qquad T_2(q^2) = \kappa A_1(q^2), \qquad T_3(q^2) = \kappa A_2(q^2)\frac{m_B^2}{q^2}, \tag{3.6}$$

where

$$\kappa = \left(1 + \frac{2D_0^{(v)}(\mu)}{C_0^{(v)}(\mu)}\right)\frac{m_b(\mu)}{m_B}. \tag{3.7}$$

Here, subleading terms of the order m_{K^*}/m_B, Λ/m_B are dropped and a naively anticommuting γ_5 matrix is used. The latter allows to relate the HQET Wilson coefficients of currents without a γ_5 matrix to those containing one by replacing $\bar{s}$ with $\bar{s}(-\gamma_5)$ in the matching equations. We also suppress the renormalization scale dependence of the penguin form factors T_i and of the coefficient κ. It reads, up to corrections of $\mathcal{O}(\alpha_s^2)$,

$$\kappa = 1 - 2\frac{\alpha_s}{3\pi}\ln\left(\frac{\mu}{m_b}\right). \tag{3.8}$$

The relations eq. (3.6) are consistent with the ones derived in [16] at lowest order in $1/m_b$ after changing to the Isgur-Wise form factor basis [20].

The inclusion of the 4-quark and gluon dipole operators leads to the effective couplings, $\mathcal{C}_{7,9}^{\text{eff}}$ [16]. They read

$$\mathcal{C}_9^{\text{eff}} = \mathcal{C}_9 + h(0, q^2) \left[\frac{4}{3}\mathcal{C}_1 + \mathcal{C}_2 + \frac{11}{2}\mathcal{C}_3 - \frac{2}{3}\mathcal{C}_4 + 52\mathcal{C}_5 - \frac{32}{3}\mathcal{C}_6 \right] \tag{3.9}$$

$$- \frac{1}{2} h(m_b, q^2) \left[7\mathcal{C}_3 + \frac{4}{3}\mathcal{C}_4 + 76\mathcal{C}_5 + \frac{64}{3}\mathcal{C}_6 \right] + \frac{4}{3} \left[\mathcal{C}_3 + \frac{16}{3}\mathcal{C}_5 + \frac{16}{9}\mathcal{C}_6 \right]$$

$$+ \frac{\alpha_s}{4\pi} \left[\mathcal{C}_1 \left(B(q^2) + 4\,C(q^2) \right) - 3\,\mathcal{C}_2 \left(2\,B(q^2) - C(q^2) \right) - \mathcal{C}_8 F_8^{(9)}(q^2) \right]$$

$$+ 8\frac{m_c^2}{q^2} \left[\frac{4}{9}\mathcal{C}_1 + \frac{1}{3}\mathcal{C}_2 + 2\,\mathcal{C}_3 + 20\,\mathcal{C}_5 \right],$$

$$\mathcal{C}_7^{\text{eff}} = \mathcal{C}_7 - \frac{1}{3} \left[\mathcal{C}_3 + \frac{4}{3}\mathcal{C}_4 + 20\,\mathcal{C}_5 + \frac{80}{3}\mathcal{C}_6 \right] + \frac{\alpha_s}{4\pi} \left[\left(\mathcal{C}_1 - 6\,\mathcal{C}_2 \right) A(q^2) - \mathcal{C}_8 F_8^{(7)}(q^2) \right], \tag{3.10}$$

and we recall that we use the 4-quark operators $\mathcal{O}_{1\dots 6}$ as defined in [22]. The functions A, B, C and $F_8^{(7)}, F_8^{(9)}$ can be seen in [30] and [14], respectively.[1] The lowest order charm loop function is given as

$$h(0, q^2) = \frac{8}{27} + \frac{4}{9} \left(\ln \frac{\mu^2}{q^2} + i\pi \right), \tag{3.11}$$

which is simply the perturbative quark loop function for massless quarks. The m_c^2/Q^2 corrections are given by the last line of eq. (3.9). Loops with b quarks stemming from penguin operators are taken into account by the function

$$h(m_b, q^2) = \frac{4}{9} \left(\ln \frac{\mu^2}{m_b^2} + \frac{2}{3} + z \right) - \frac{4}{9}(2 + z)\sqrt{z - 1} \arctan \frac{1}{\sqrt{z-1}}, \quad z = \frac{4m_b^2}{q^2}. \tag{3.12}$$

We stress that the effective coefficients eqs. (3.9)–(3.10) are different from the ones used in the low q^2 region given in [14].

The product $m_b\,\kappa\,\mathcal{C}_7^{\text{eff}}$ is independent of the renormalization scale [16]. As we will see in the next section, this is important because contributions from $\mathcal{C}_7^{\text{eff}}$ enter the $\bar{B} \to \bar{K}^* l^+ l^-$ amplitudes in exactly this combination. The μ-dependence of $\mathcal{C}_9^{\text{eff}}$ is very small and induced at the order $\alpha_s^2\,\mathcal{C}_{1,2}$ and $\alpha_s\,\mathcal{C}_{3,\dots 6}$.

The heavy quark matrix elements $\langle K^* | \bar{s}i\overleftarrow{D}_\mu(\gamma_5)h_v | B \rangle$ are the only new hadronic input required at order Λ/m_b for both the form factor relations and the matrix elements related to the electromagnetic current, $\mathcal{C}_{7,9}^{\text{eff}}$ [16]. However, we refrain from including these explicit Λ/m_b corrections. Firstly, the requisite additional matrix elements are currently only known from constituent quark model calculations [19, 33] bringing in sizable uncertainties. More importantly, the leading power corrections to the form factor relations are parametrically suppressed, see section 3.2. Note that the ones to the OPE arise only at $\mathcal{O}(\alpha_s \Lambda/m_b, m_c^4/Q^4)$. Hence, the power corrections have a reduced impact on the decay observables. Quantitative estimates are given in section 4.1.

Note that explicit spectator effects are power suppressed and absent to the order we are working. They only appear indirectly in the form factors, lifetime and meson

---

[1]Note that in [30] a different sign convention has been used than in the previous works [31, 32].

masses. Hence, the formulae can be used for charged and neutral $\bar{B} \to \bar{K}^* l^+ l^-$ decays, and $\bar{B}_s \to \phi l^+ l^-$ decays after the necessary replacements.

3.2 The transversity amplitudes

Application of the form factor relations in eq. (3.6) and using the effective coefficients eqs. (3.9)–(3.10) yields the low recoil transversity amplitudes to leading order in $1/m_b$ as

$$A_\perp^{L,R} = +i \left\{ (\mathcal{C}_9^{\text{eff}} \mp \mathcal{C}_{10}) + \kappa \frac{2\hat{m}_b}{\hat{s}} \mathcal{C}_7^{\text{eff}} \right\} f_\perp, \tag{3.13}$$

$$A_\parallel^{L,R} = -i \left\{ (\mathcal{C}_9^{\text{eff}} \mp \mathcal{C}_{10}) + \kappa \frac{2\hat{m}_b}{\hat{s}} \mathcal{C}_7^{\text{eff}} \right\} f_\parallel, \tag{3.14}$$

$$A_0^{L,R} = -i \left\{ \left(\mathcal{C}_9^{\text{eff}} \mp \mathcal{C}_{10} \right) + \kappa \frac{2\hat{m}_b}{\hat{s}} \mathcal{C}_7^{\text{eff}} \right\} f_0, \tag{3.15}$$

where the form factors enter as

$$f_\perp = N m_B \frac{\sqrt{2\hat{\lambda}}}{1 + \hat{m}_{K^*}} V, \qquad\qquad f_\parallel = N m_B \sqrt{2} \left(1 + \hat{m}_{K^*} \right) A_1,$$

$$f_0 = N m_B \frac{(1 - \hat{s} - \hat{m}_{K^*}^2)(1 + \hat{m}_{K^*})^2 A_1 - \hat{\lambda} A_2}{2 \hat{m}_{K^*}(1 + \hat{m}_{K^*})\sqrt{\hat{s}}}, \tag{3.16}$$

and the normalization factor reads

$$N = \sqrt{\frac{G_F^2 \alpha_e^2 |\lambda_t|^2 m_B \hat{s} \sqrt{\hat{\lambda}}}{3 \cdot 2^{10} \pi^5}}. \tag{3.17}$$

Here, we switched to the dimensionless variables $\hat{s} = q^2/m_B^2$, $\hat{m}_i = m_i/m_B$ and $\hat{\lambda} = 1 + \hat{s}^2 + \hat{m}_{K^*}^4 - 2(\hat{s} + \hat{s}\hat{m}_{K^*}^2 + \hat{m}_{K^*}^2)$. We also suppressed for brevity the dependence on the momentum transfer in the form factors and the effective coefficients. We further neglected subleading terms of order m_{K^*}/m_B in the $\mathcal{C}_7^{\text{eff}}$-term only.

Interestingly, within our framework (SM basis, lowest order in Λ/m_b) the transversity amplitudes eqs. (3.13)–(3.15) depend in exactly the same way on the short distance coefficients. Consequently, only two independent combinations of Wilson coefficients can be probed, related to $|A_i^L|^2 \pm |A_i^R|^2$, since A^L and A^R do not interfere for massless leptons, see appendix A. The independent combinations can be defined as

$$\rho_1 \equiv \left| \mathcal{C}_9^{\text{eff}} + \kappa \frac{2\hat{m}_b}{\hat{s}} \mathcal{C}_7^{\text{eff}} \right|^2 + |\mathcal{C}_{10}|^2, \tag{3.18}$$

$$\rho_2 \equiv \text{Re}\left\{ \left(\mathcal{C}_9^{\text{eff}} + \kappa \frac{2\hat{m}_b}{\hat{s}} \mathcal{C}_7^{\text{eff}} \right) \mathcal{C}_{10}^* \right\}. \tag{3.19}$$

ρ_1 and ρ_2 are largely μ-scale independent. The dominant dependence on the dilepton mass in $\rho_{1,2}$ stems from the $1/\hat{s}$-factor accompanying $\mathcal{C}_7^{\text{eff}}$. The short distance parameter ρ_1 equals up to Λ/m_b corrections the parameter N_{eff} introduced in ref. [16].

The relation between all three transversity amplitudes makes the low recoil region overconstrained and very predictive. We work out the corresponding implications in section 3.3. Note that in the large recoil region two amplitudes are related as $A_\parallel^X = -A_\perp^X$ by helicity conservation up to corrections in $1/E_{K^*}$ in the SM basis [34].

The leading power corrections of the OPE arise at $\mathcal{O}(\alpha_s \Lambda/m_b, m_c^4/Q^4) \sim$ few percent. The Λ/m_b corrections to the amplitudes from the form factor relations are parametrically suppressed as well, by small dipole coefficients, such that we can estimate the leading power correction from the form factor relations to the decay amplitudes as order $(2\mathcal{C}_7^{\rm eff}/\mathcal{C}_9^{\rm eff})\Lambda/m_b$. So in general, the dominant power corrections to the transversity amplitudes are of the order few percent.

We simulate the effect of the $1/m_b$ corrections by dimensional analysis when estimating theoretical uncertainties in section 4.1.

3.3 Observables and predictions

We begin with low recoil predictions of some basic distributions. At leading order they can be written in terms of the transversity amplitudes $A_{\perp,\parallel,0}$ given in eqs. (3.13)–(3.15) as:

$$\frac{d\Gamma}{dq^2} = 2\,\rho_1 \times (f_0^2 + f_\perp^2 + f_\parallel^2), \tag{3.20}$$

$$A_{\rm FB} = 3\,\frac{\rho_2}{\rho_1} \times \frac{f_\perp f_\parallel}{(f_0^2 + f_\perp^2 + f_\parallel^2)}, \tag{3.21}$$

$$F_{\rm L} = \frac{f_0^2}{f_0^2 + f_\perp^2 + f_\parallel^2}, \tag{3.22}$$

and

$$A_T^{(2)} = \frac{f_\perp^2 - f_\parallel^2}{f_\perp^2 + f_\parallel^2}, \qquad A_T^{(3)} = \frac{f_\parallel}{f_\perp}, \qquad A_T^{(4)} = 2\,\frac{\rho_2}{\rho_1} \times \frac{f_\perp}{f_\parallel}. \tag{3.23}$$

The new high q^2 transversity observables read as

$$H_T^{(1)} = 1, \qquad\qquad H_T^{(2)} = H_T^{(3)} = 2\,\frac{\rho_2}{\rho_1}. \tag{3.24}$$

All observables factorize into short distance coefficients $\rho_{1,2}$ and form factor ones $f_{0,\perp,\parallel}$.

We note the following:

- The only two independent combinations of Wilson coefficients, ρ_1 and ρ_2, enter the decay rate $d\Gamma/dq^2$ and the forward-backward asymmetry $A_{\rm FB}$, respectively.

- The observables $F_{\rm L}$, $A_T^{(2,3)}$ and $H_T^{(1)}$ are independent of the Wilson coefficients. Data on $F_{\rm L}$ and $A_T^{(2,3)}$ test the form factors. In particular, $A_T^{(2)}$ and $A_T^{(3)}$ each measure the ratio A_1/V, whereas $F_{\rm L}$ is in addition sensitive to A_2. More observables designed to not depend on the short distance coefficients are given in appendix B, see eq. (B.10).

- More generally, in the SM basis and to the order we are working, any observable in the decay $\bar{B} \to \bar{K}^*(\to \bar{K}\pi)l^+l^-$ is correlated with $d\Gamma/dq^2$ or $A_{\rm FB}$, or is independent of the Wilson coefficients. Data on the multitude of angular observables can hence be used to test our framework, that is, whether there are further operators beyond eq. (2.2), the goodness of the OPE, and the form factors.

$\lvert V_{tb}V_{ts}^*\rvert$	0.0409 ± 0.0013		$\alpha_s(M_Z)$	0.1176 ± 0.0020	[35]
$\lvert V_{cb}\rvert$	0.0417 ± 0.0013		$\alpha_e(m_b)$	$1/133$	
$\lvert V_{ub}\rvert/\lvert V_{tb}V_{ts}^*\rvert$	$0.0884^{+0.064}_{-0.054}$		τ_{B^0}	(1.530 ± 0.009) ps	[35]
$m_c(m_c)$	$(1.27^{+0.07}_{-0.11})$ GeV	[35]	f_{B^0}	(200 ± 30) MeV	
$m_b(m_b)$	(4.2 ± 0.17) GeV	[35]	$f_\parallel^{K^*}$	(217 ± 5) MeV	
m_t^{pole}	(173.1 ± 1.3) GeV	[36]	$f_\perp^{K^*}(1\,\text{GeV})$	(185 ± 10) MeV	
M_W	(80.398 ± 0.025) GeV	[35]	$\lambda_{B,+}(1.5\,\text{GeV})$	(0.458 ± 0.115) GeV	[15]
M_Z	(91.1876 ± 0.0021) GeV	[35]	$a_{1,K^*}^{\parallel,\perp}$	(0.1 ± 0.07) MeV	[37]
$\mathcal{B}(\bar B \to X_c l\bar\nu_l)$	(10.5 ± 0.4) %	[35]	$a_{2,K^*}^{\parallel,\perp}$	(0.1 ± 0.1) MeV	[37]

Table 1. The numerical input used in our analysis. We neglect the mass of the strange quark. τ_{B^0} denotes the lifetime of the neutral B meson.

- The $H_T^{(1,2,3)}$, by construction, do not depend on the form factors. Within our framework, these are the only observables with this feature, see appendix B.

- Moreover, $H_T^{(1)}$ does not depend on Wilson coefficients either. Its simple prediction eq. (3.24) holds beyond the SM and provides a null test of the framework.

- The set of observables eqs. (3.20)–(3.24) and (B.10) with two short distance and three form factor coefficients is heavily overconstrained. Measurements can directly yield either products $\rho_i f_j f_k$ or ratios ρ_2/ρ_1 and f_j/f_k, but not the f_i or the ρ_i alone.

4 Exploiting data

We give numerical SM predictions for $\bar B \to \bar K^* l^+ l^-$ decay observables in section 4.1, with emphasis on the low recoil region. In section 4.2 we confront the distributions with existing data and work out constraints for the Wilson coefficients. Next, we combine low with large recoil regions and point out complementarities.

4.1 SM predictions

The low recoil predictions are obtained using the formulae given in section 3. The framework applies to the region where the $\bar K^*$ is soft in the heavy mesons rest frame, i.e., has energy $E_{K^*} = m_{K^*} + \Lambda$. In terms of dilepton masses, this corresponds to large values, $q^2 \gtrsim (m_B - m_{K^*})^2 - 2m_B\Lambda$ up to the kinematical endpoint. We use, unless otherwise stated,

$$q^2_{\min} = 14\,\text{GeV}^2 < q^2 \leq 19.2\,\text{GeV}^2 = q^2_{\max}, \tag{4.1}$$

obtained numerically for $\Lambda = 500\,\text{MeV}$, with the lower boundary starting just above the ψ' resonance.

To make quantitative predictions in the low recoil region the $B \to K^*$ form factors are requisite input. Unfortunately, the current knowledge on the form factors at low recoil is very limited and our results can as far as form factor uncertainties are concerned provide guidance of the achievable precision only.

For our numerics we use the light cone sum rule (LCSR) results of ref. [37] extrapolated from their domain of validity at large recoil to the low recoil one with physical pole or dipole shapes. These extrapolations are supported by fits based on series expansion in the case of $B \to K$ and $B \to \rho$ transitions [38]. Note that there is lattice and experimental information available on $B \to \rho$ form factors at low recoil [39, 40], however, to use this for $B \to K^*$ would require knowledge of the size of SU(3) flavor breaking. More details on the form factors and a comparison with existing lattice results for $T_{1,2}$ [41, 42] are given in appendix C. We use the parameters given in table 1.

From q^2-integration in the low recoil region eq. (4.1) we obtain the integrated SM branching ratio $\mathrm{d}\mathcal{B}/\mathrm{d}q^2 = \tau_B \mathrm{d}\Gamma/\mathrm{d}q^2$ as

$$10^7 \cdot \int_{q_{\min}^2}^{q_{\max}^2} \mathrm{d}q^2 \frac{\mathrm{d}\mathcal{B}}{\mathrm{d}q^2} = 2.96 \,{}^{+0.90}_{-0.77}\Big|_{\mathrm{FF}} \,{}^{+0.18}_{-0.17}\Big|_{\mathrm{SL}} \pm 0.10\Big|_{\mathrm{IWR}} \pm 0.16\Big|_{\mathrm{CKM}} \,{}^{+0.08}_{-0.06}\Big|_{\mathrm{SD}}. \tag{4.2}$$

For the remaining q^2-distributions X of eqs. (2.8)–(2.15) we define "naively integrated" observables as

$$\overline{X} \equiv \frac{1}{q_{\max}^2 - q_{\min}^2} \int_{q_{\min}^2}^{q_{\max}^2} \mathrm{d}q^2 X(q^2). \tag{4.3}$$

For these we obtain

$$\overline{A_{\mathrm{FB}}} = -0.39 \,{}^{+0.06}_{-0.07}\Big|_{\mathrm{FF}} \pm 0.02\Big|_{\mathrm{SL}} \pm 0.01\Big|_{\mathrm{IWR}} \pm 0.001\Big|_{\mathrm{SD}}, \tag{4.4}$$

$$\overline{F_{\mathrm{L}}} = 0.35 \,{}^{+0.03}_{-0.04}\Big|_{\mathrm{FF}} \pm 0.03\Big|_{\mathrm{SL}} \pm 0.01\Big|_{\mathrm{IWR}}, \tag{4.5}$$

$$\overline{A_T^{(2)}} = -0.54 \,{}^{+0.15}_{-0.13}\Big|_{\mathrm{FF}} \,{}^{+0.04}_{-0.03}\Big|_{\mathrm{SL}} \,{}^{+0.03}_{-0.02}\Big|_{\mathrm{IWR}}, \tag{4.6}$$

$$\overline{A_T^{(3)}} = +2.25 \,{}^{+0.52}_{-0.45}\Big|_{\mathrm{FF}} \pm 0.11\Big|_{\mathrm{SL}} \pm 0.08\Big|_{\mathrm{IWR}}, \tag{4.7}$$

$$\overline{A_T^{(4)}} = +0.53 \,{}^{+0.12}_{-0.11}\Big|_{\mathrm{FF}} \pm 0.03\Big|_{\mathrm{SL}} \pm 0.02\Big|_{\mathrm{IWR}} \pm 0.002\Big|_{\mathrm{SD}}, \tag{4.8}$$

$$\overline{H_T^{(1)}} = +1.000 \,{}^{+0}_{-0.00002}\Big|_{\mathrm{SL}} \,{}^{+0}_{-0.0007}\Big|_{\mathrm{IWR}}, \tag{4.9}$$

$$\overline{H_T^{(2,3)}} = -0.985 \pm 0.001\Big|_{\mathrm{SL}} \,{}^{+0.007}_{-0.005}\Big|_{\mathrm{IWR}} \,{}^{+0.004}_{-0.003}\Big|_{\mathrm{SD}}. \tag{4.10}$$

In addition, we consider the integrated observables $\langle X \rangle$ defined by replacing J_i with its integral $\langle J_i \rangle$ in each of the observables $X = X(J_i)$ in eqs. (2.7)–(2.15),

$$\langle X \rangle \equiv X(\langle J_i \rangle), \qquad \langle J_i \rangle \equiv \int_{q_{\min}^2}^{q_{\max}^2} \mathrm{d}q^2 J_i(q^2). \tag{4.11}$$

This definition agrees with the way $\mathcal{B}, A_{\mathrm{FB}}$ and F_{L} are obtained experimentally [11–13], i.e., by integrating numerator and denominator before taking the ratio. Using the same

integration boundaries as above, eq. (4.1), we obtain

$$\langle A_{\mathrm{FB}} \rangle = -0.41 \pm 0.07 \Big|_{\mathrm{FF}} \pm 0.02 \Big|_{\mathrm{SL}} \pm 0.01 \Big|_{\mathrm{IWR}} {}^{+0.001}_{-0.002} \Big|_{\mathrm{SD}}, \tag{4.12}$$

$$\langle F_{\mathrm{L}} \rangle = 0.35 {}^{+0.04}_{-0.05} \Big|_{\mathrm{FF}} \pm 0.03 \Big|_{\mathrm{SL}} \pm 0.02 \Big|_{\mathrm{IWR}}, \tag{4.13}$$

$$\langle A_T^{(2)} \rangle = -0.48 {}^{+0.18}_{-0.15} \Big|_{\mathrm{FF}} {}^{+0.04}_{-0.04} \Big|_{\mathrm{SL}} \pm 0.03 \Big|_{\mathrm{IWR}} \pm 0.001 \Big|_{\mathrm{SD}}, \tag{4.14}$$

$$\langle A_T^{(3)} \rangle = 1.71 {}^{+0.39}_{-0.33} \Big|_{\mathrm{FF}} \pm 0.08 \Big|_{\mathrm{SL}} \pm 0.06 \Big|_{\mathrm{IWR}} \pm 0.001 \Big|_{\mathrm{SD}}, \tag{4.15}$$

$$\langle A_T^{(4)} \rangle = 0.58 {}^{+0.13}_{-0.11} \Big|_{\mathrm{FF}} {}^{+0.09}_{-0.09} \Big|_{\mathrm{SL}} \pm 0.07 \Big|_{\mathrm{IWR}} \pm 0.002 \Big|_{\mathrm{SD}}, \tag{4.16}$$

$$\langle H_T^{(1)} \rangle = +0.997 \pm 0.002 \Big|_{\mathrm{FF}} {}^{+0}_{-0.001} \Big|_{\mathrm{IWR}}, \tag{4.17}$$

$$\langle H_T^{(2)} \rangle = -0.972 {}^{+0.004}_{-0.003} \Big|_{\mathrm{FF}} \pm 0.001 \Big|_{\mathrm{SL}} {}^{+0.008}_{-0.005} \Big|_{\mathrm{IWR}} {}^{+0.003}_{-0.004} \Big|_{\mathrm{SD}}, \tag{4.18}$$

$$\langle H_T^{(3)} \rangle = -0.958 \pm 0.001 \Big|_{\mathrm{SL}} {}^{+0.008}_{-0.006} \Big|_{\mathrm{IWR}} {}^{+0.003}_{-0.004} \Big|_{\mathrm{SD}}, \tag{4.19}$$

with the branching ratio as before, eq. (4.2). Uncertainties not explicitly given are below $\mathcal{O}(10^{-4})$.

In both definitions of integrated observables the uncertainties are estimated the same way: The dominant uncertainty of the form factors V, A_1 and A_2 has been assumed $\pm 15\,\%$ (FF). Furthermore, we include a real scaling factor for each of the transversity amplitudes $A_{\perp,\parallel,0}^{L,R}$ in order to estimate uncertainties due to the subleading corrections of order $\alpha_s \Lambda/m_b$ by varying them with $\pm 5\,\%$ (SL). The subleading corrections to the improved Isgur-Wise form factor relations eq. (3.6), of order Λ/m_b, and the neglected kinematical factors of m_{K^*}/m_B in the term $\sim \kappa \mathcal{C}_7^{\mathrm{eff}}$ are accounted for by three real scale factors for $A_{\perp,\parallel,0}$ with $\pm 20\,\%$ (IWR). Note however, that the latter are additionally suppressed in the SM by $2\mathcal{C}_7^{\mathrm{eff}}/\mathcal{C}_9^{\mathrm{eff}}$. The uncertainties due to the CKM parameters $V_{tb}V_{ts}^*$ correspond to their 1σ ranges (CKM), which cancel in the normalized quantities and thus appear in the branching ratio only. The uncertainties due to the μ-dependence and the t- and b-quark masses (at 1σ) concern the short distance couplings $\rho_{1,2}$ only, and are subsumed under the label (SD). The variation with the scale $\mu \in [\mu_b/2, 2\mu_b]$ (with central value $\mu_b = 4.2$ GeV) is small, as expected.

In figure 1 we show ρ_1 and the ratio ρ_2/ρ_1 with error bands from different sources. The t-pole mass and b-$\overline{\mathrm{MS}}$ mass dependence (at 3σ) are comparable in size and amount to about 5 % each. Finally, a variation of $\pm 20\,\%$ due to the subleading Λ/m_b and m_{K^*}/m_B corrections denoted above as (IWR) results in about 6 % uncertainty. The overall uncertainty of ρ_1 and ρ_2 is about 9 % and 10 %, respectively, when adding all uncertainties in quadrature. However, the uncertainties cancel to a large extent in the ratio ρ_2/ρ_1, providing a strong test of the SM when measuring the observables $H_T^{(2,3)}$ [eqs. (2.14)–(2.15)] with an uncertainty of about 2 % (at 3σ).

The uncertainties of each group (FF), (SL), (IWR), (CKM) and (SD) are obtained by varying each parameter separately and adding them subsequently in quadrature. Our SM values for $\langle A_{\mathrm{FB}} \rangle$ and $\langle F_{\mathrm{L}} \rangle$ are in agreement with [43].
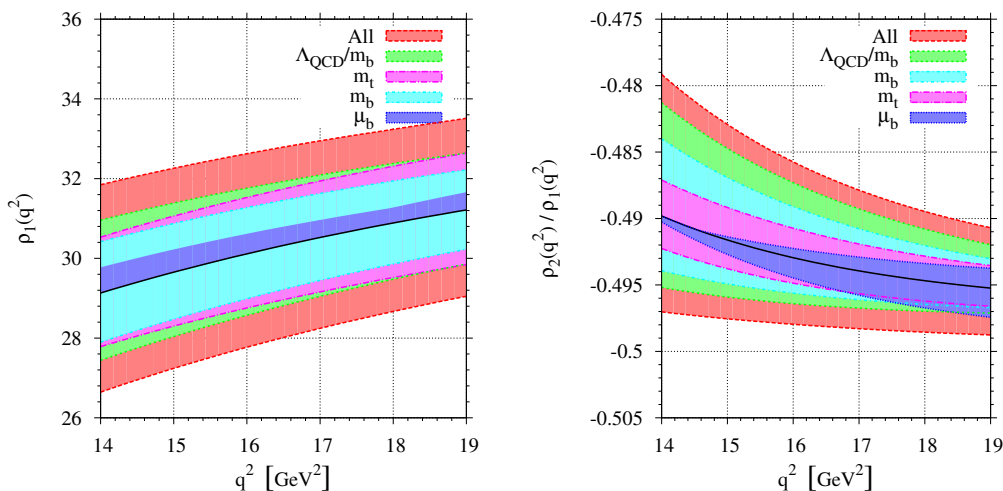
Figure 1. The short distance coupling ρ_1 and the ratio ρ_2/ρ_1 in the SM.

For the SM predictions at large recoil [14, 15] we follow closely [17], with the updates of the numerical input given in table 1. In this kinematical region, spectator effects arise and for concreteness, we give predictions for neutral $\bar{B}$ decays.

We estimate the uncertainties due to the two large energy form factors $\xi_{\perp,\parallel}$ by varying them separately — for an improved treatment of this source of uncertainty using directly the LCSRs the reader is refered to [26]. Furthermore, we estimate uncertainties due to subleading QCDF corrections of order Λ/m_b by varying a real scale factor for each of the transversity amplitudes $A_{\perp,\parallel,0}^{L,R}$ within ± 10 % separately and adding the resulting uncertainties subsequently in quadrature. The latter constitute the numerically leading uncertainties in the observables $A_T^{(2,3,4)}$ where form factor uncertainties cancel at leading order in QCDF [25].

The differential branching ratio $\mathrm{d}\mathcal{B}/\mathrm{d}q^2$, the forward-backward asymmetry A_{FB} and the longitudinal polarization F_{L} in the SM in both the low and large recoil regions are shown in figure 2. The vertical grey bands are the regions vetoed by the experiments to remove backgrounds from intermediate charmonia, J/ψ and ψ' decaying to muon pairs for $8.68\,\mathrm{GeV}^2 < q^2 < 10.09\,\mathrm{GeV}^2$ and $12.86\,\mathrm{GeV}^2 < q^2 < 14.18\,\mathrm{GeV}^2$ [12, 13]. Within QCDF, the region of validity is approximately within $(1-7)\,\mathrm{GeV}^2$. We mark the large recoil range (below the J/ψ) outside this range by dashed lines.

In figure 3 we show the SM predictions for $\mathcal{B}, A_{\mathrm{FB}}$ and F_{L} next to the available data. Note that the physical region of F_{L} is between 0 and 1. The data are consistent with the SM, although they allow for large deviations from the SM as well given the sizeable uncertainties. In particular, the data for $\mathcal{B}$ at low q^2 and A_{FB} at high q^2 show a trend to be slighly below the SM. The shape of A_{FB} at low q^2 is currently not settled and allows for either sign of the dipole coefficient $\mathcal{C}_7$ while having the others kept at their SM values. In the future the LHCb collaboration expects to surpass the precision of the existing B-factory A_{FB} measurements after an integrated luminosity of $0.3\,\mathrm{fb}^{-1}$ [44], and may shed light on this matter.

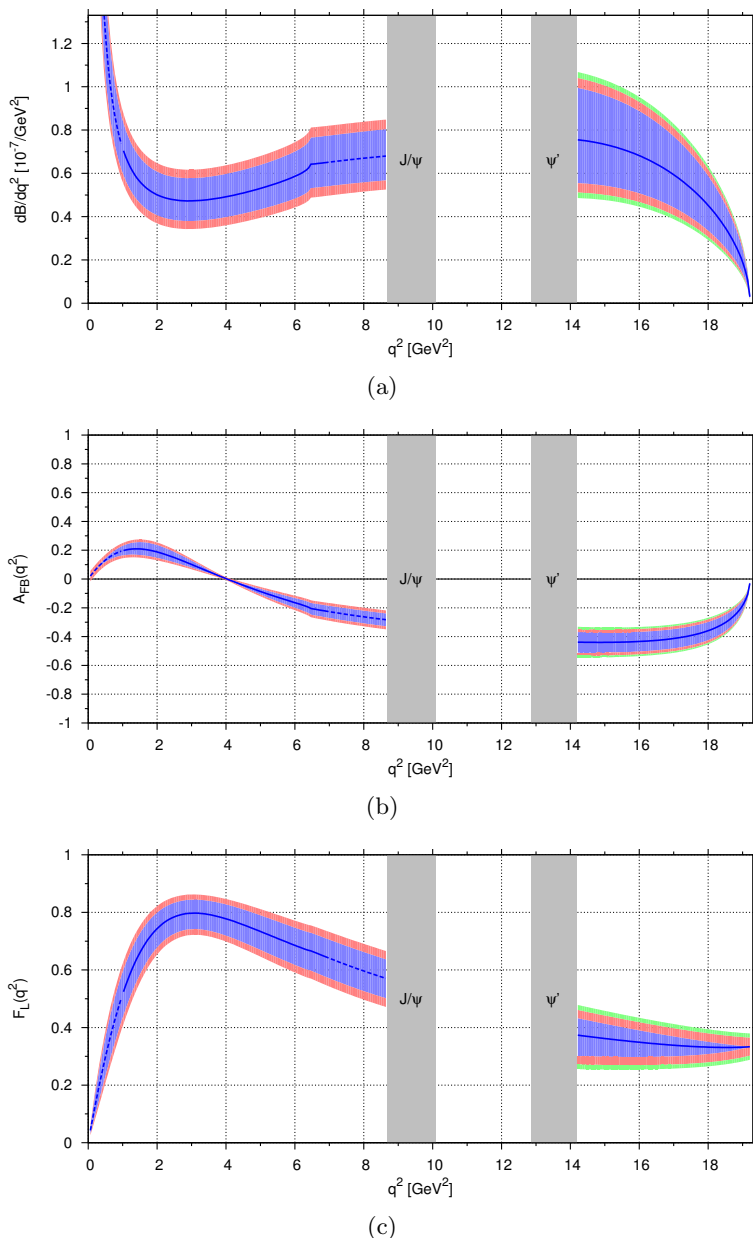**Figure 2**. The differential branching ratio $d\mathcal{B}/dq^2$ in units of $10^{-7}/\text{GeV}^2$ (a), the forward-backward asymmetry A_{FB} (b) and the longitudinal polarization F_{L} (c) in the large recoil $q^2 < m_{J/\psi}^2$ and the low recoil $q^2 \gtrsim m_{\psi'}^2 \sim \mathcal{O}(m_b^2)$ regions in the SM. At low recoil, the uncertainties shown are due to the Λ/Q expansion of the improved Isgur-Wise relations (green bands), subleading terms of order $\alpha_s \Lambda/Q$ (red bands) and the form factors (blue bands). At large recoil, the bands denote the uncertainties from Λ/m_b, Λ/E_{K^*} corrections (red bands) and the form factors (blue bands). The vertical shaded (grey) bands mark the experimental veto regions [12, 13] to remove contributions from $\bar{B} \to J/\psi(\to \mu^+\mu^-)\bar{K}^*$ (left band) and $\bar{B} \to \psi'(\to \mu^+\mu^-)\bar{K}^*$ (right band).

In figure 4 we show $A_T^{(2,3,4)}$ in the SM. The behaviour in the low and high q^2 region is very different from each other. In particular, $A_T^{(2)}$ is strongly suppressed, in fact, vanishes
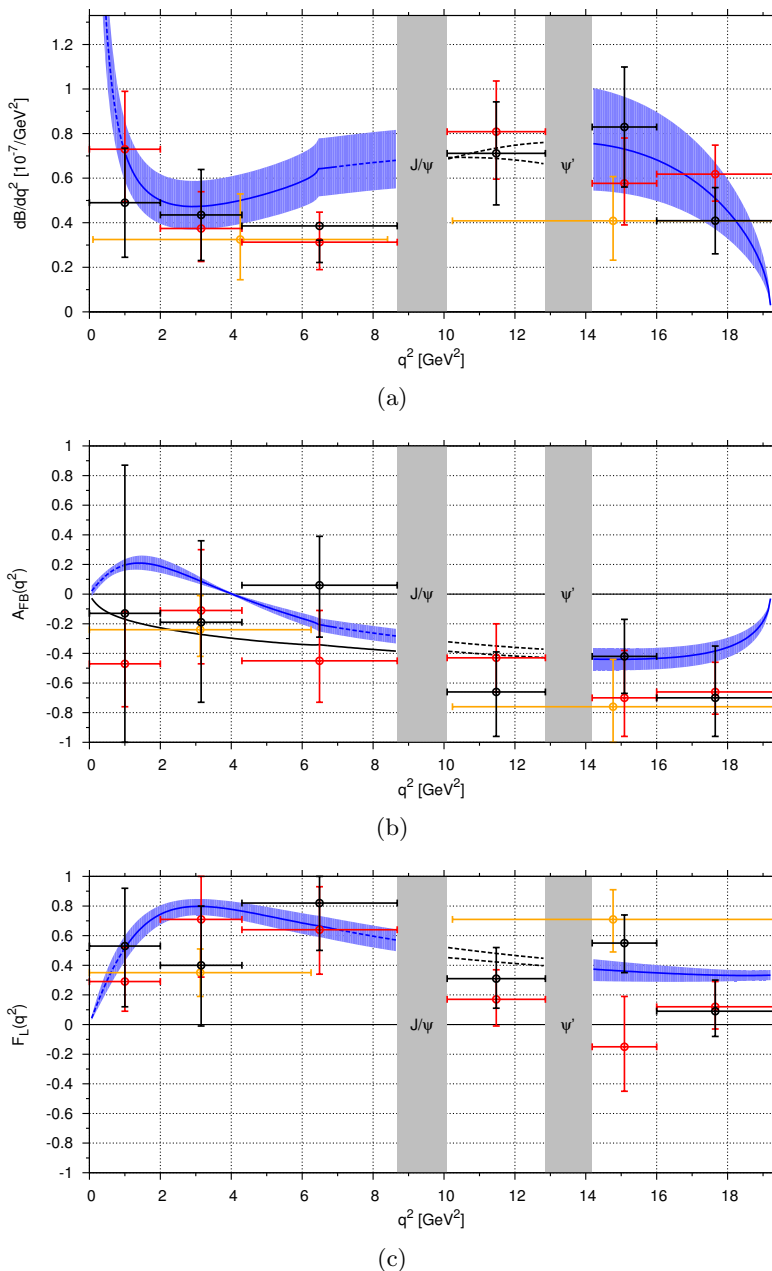
Figure 3. The $\bar{B} \to \bar{K}^* l^+ l^-$ distributions $\mathrm{d}\mathcal{B}/\mathrm{d}q^2$ (a), A_{FB} (b) and F_{L} (c) in the SM including the theoretical uncertainties added in quadrature (shaded blue bands) versus the existing data from Belle [12] (red), BaBar [10, 11] (gold) and CDF [13] (black). The experimental data for A_{FB} have their sign flipped to match the conventions used in this work. The isolated solid (black) line in the A_{FB} plot illustrates the case with $\mathcal{C}_7 = -\mathcal{C}_7^{\mathrm{SM}}$. The vertical shaded (grey) bands are defined as in figure 2. The isolated dashed (black) lines between the $\bar{c}c$-bands are theory extrapolations from the low and large recoil region.

up to $1/E_{K^*}$ corrections by helicity conservation [34] for low dilepton masses, but is order one for large ones. The size of $A_T^{(2)}$ at low q^2 can be used as an indicator for the correctness
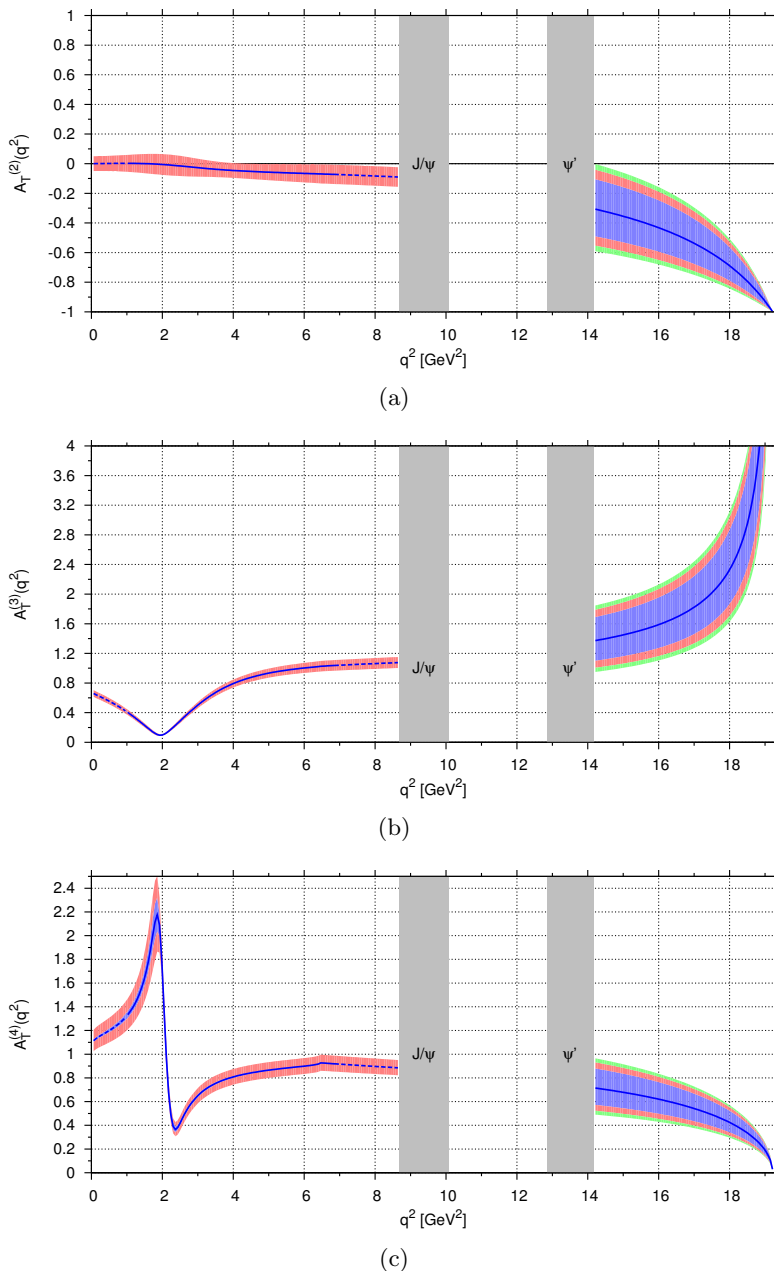
Figure 4. The transverse asymmetries $A_T^{(2)}$ (a), $A_T^{(3)}$ (b) and $A_T^{(4)}$ (c) in the SM. The explanation of the bands is the same as in figure 2.

of our assumptions: in the presence of chirality-flipped operators beyond those in eq. (2.2), the aforementioned suppression of $A_T^{(2)}$ would be lifted. Note that $A_T^{(3)}$ is proportional to $1/\sqrt{\hat{\lambda}}$ and diverges at the endpoint $\hat{\lambda} \to 0$. On the other hand, $A_T^{(4)} \propto \sqrt{\hat{\lambda}}$ is finite in this limit and vanishes at maximum q^2.

The q^2-behaviour of both the new, transverse observables $H_T^{(2,3)}$ can be obtained from figure 1, where ρ_2/ρ_1 is shown in the SM.
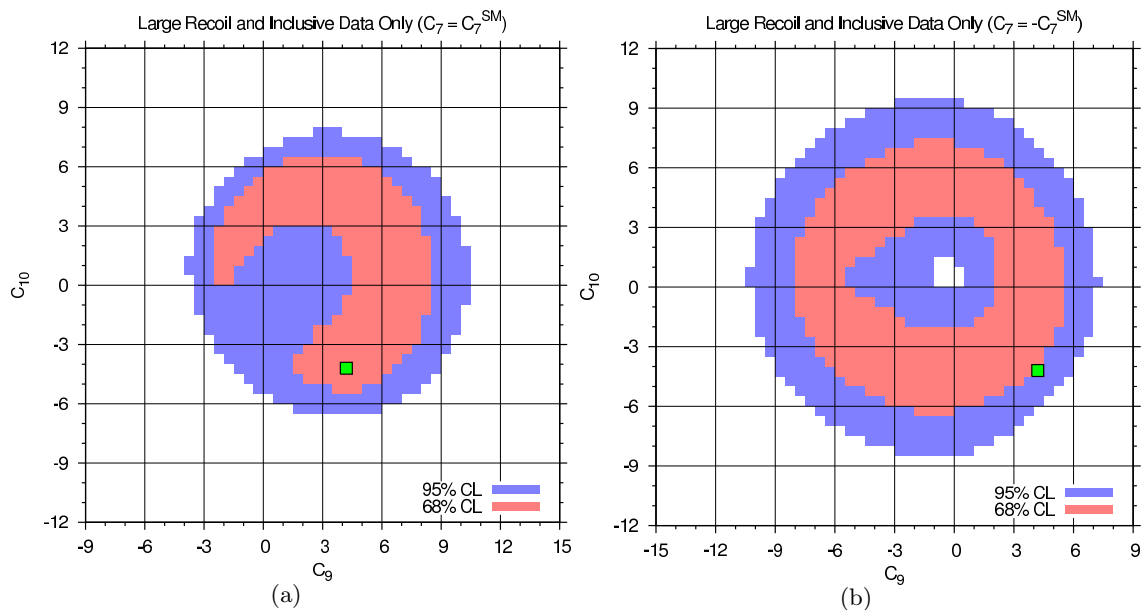
Figure 5. The constraints on $\mathcal{C}_9$ and $\mathcal{C}_{10}$ from $\bar{B} \to \bar{K}^* l^+ l^-$ at large recoil and $\bar{B} \to X_s l^+ l^-$ for $\mathcal{C}_7 = \mathcal{C}_7^{\mathrm{SM}}$ (a) and $\mathcal{C}_7 = -\mathcal{C}_7^{\mathrm{SM}}$ (b) using Belle [12, 48], BaBar [49] and CDF [13] data at 68% CL (red areas) and 95% CL (red and blue areas). The (green) square marks the SM value of $(\mathcal{C}_9, \mathcal{C}_{10})$.
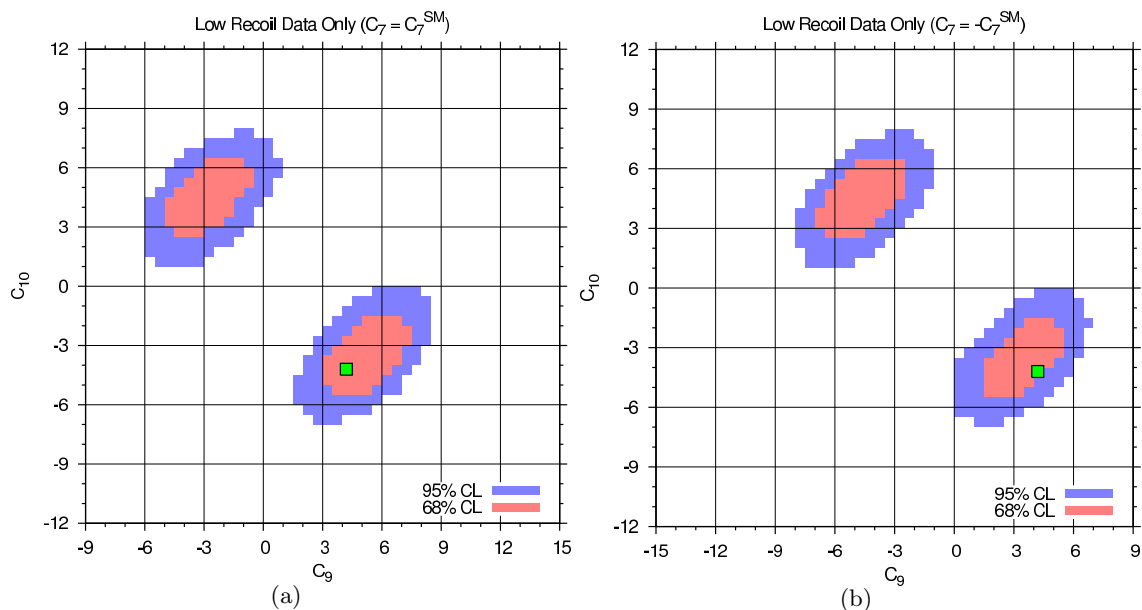

Figure 6. The constraints on $\mathcal{C}_9$ and $\mathcal{C}_{10}$ from $\bar{B} \to \bar{K}^* l^+ l^-$ low recoil data [12, 13] only for $\mathcal{C}_7 = \mathcal{C}_7^{\mathrm{SM}}$ (a) and $\mathcal{C}_7 = -\mathcal{C}_7^{\mathrm{SM}}$ (b) at 68% CL (red areas) and 95% CL (red and blue areas). The (green) square marks the SM value of $(\mathcal{C}_9, \mathcal{C}_{10})$.
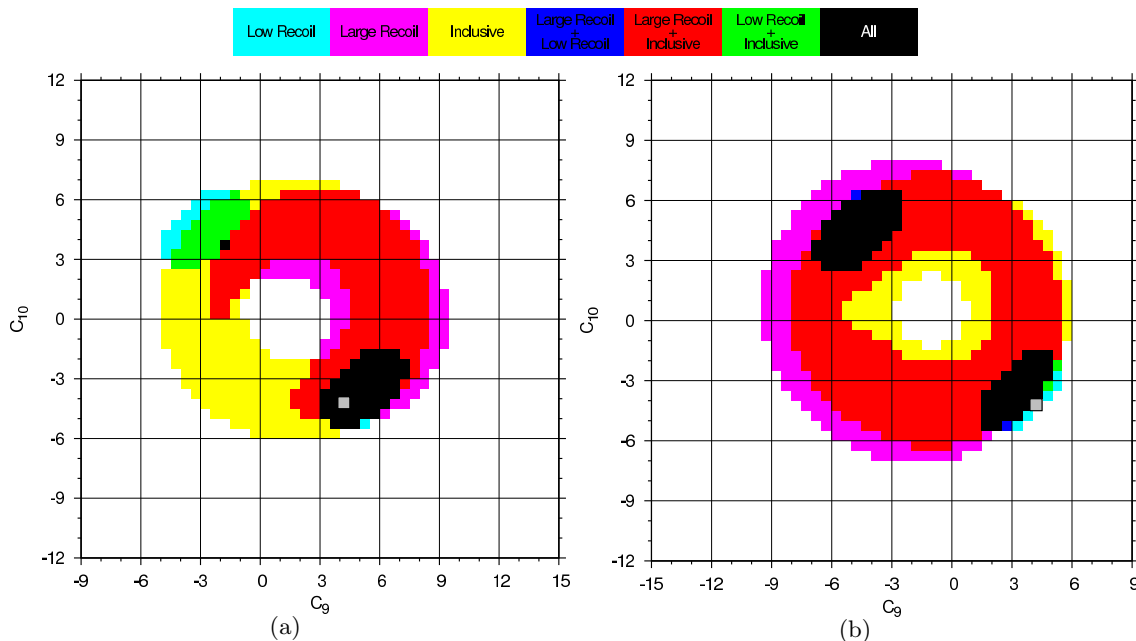
Figure 7. The individual 68% CL constraints on $\mathcal{C}_9$ and $\mathcal{C}_{10}$ from $\bar{B} \to \bar{K}^* l^+ l^-$ at large and low recoil and $\bar{B} \to X_s l^+ l^-$ for $\mathcal{C}_7 = \mathcal{C}_7^{\mathrm{SM}}$ (a) and $\mathcal{C}_7 = -\mathcal{C}_7^{\mathrm{SM}}$ (b) using Belle [12, 48], BaBar [49] and CDF [13] data. The (grey) square marks the SM value of $(\mathcal{C}_9, \mathcal{C}_{10})$. See the color key at the top for the different constraints.
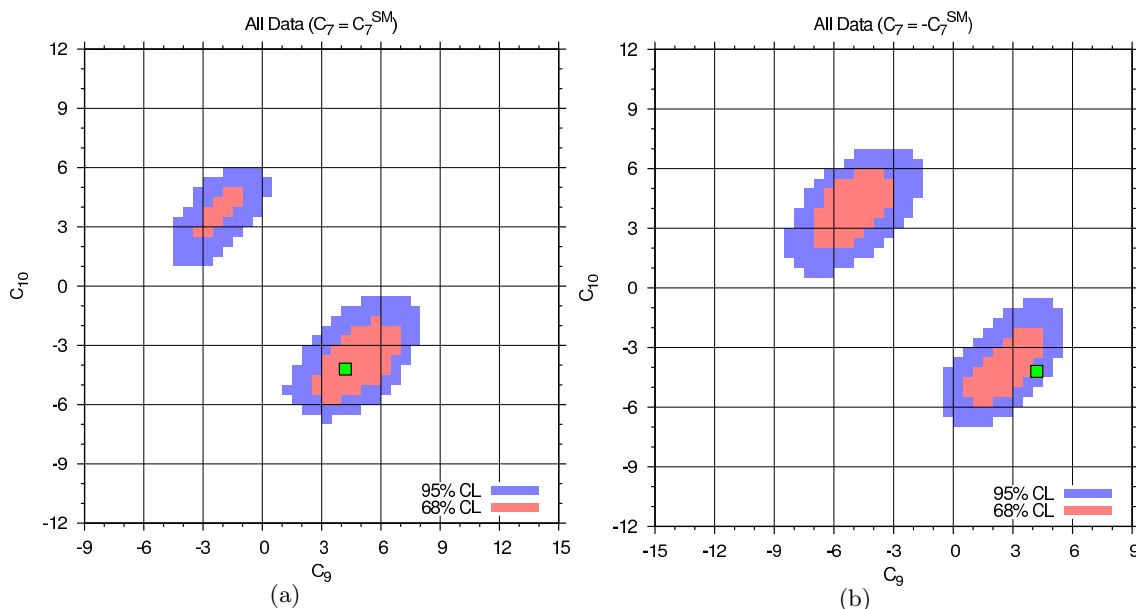

Figure 8. The global constraints on $\mathcal{C}_9$ and $\mathcal{C}_{10}$ from $\bar{B} \to \bar{K}^* l^+ l^-$ and $\bar{B} \to X_s l^+ l^-$ for $\mathcal{C}_7 = \mathcal{C}_7^{\mathrm{SM}}$ (a) and $\mathcal{C}_7 = -\mathcal{C}_7^{\mathrm{SM}}$ (b) using Belle [12, 48], BaBar [49] and CDF [13] data at 68% CL (red area) and 95% CL (red and blue areas). The (green) square marks the SM value of $(\mathcal{C}_9, \mathcal{C}_{10})$.

4.2 Constraining new physics

To confront the available data with the SM we perform a parameter scan over $-15 \leq \mathcal{C}_{9,10} \leq 15$ for 60×60 points and check the goodness-of-fit for each of the observables listed in table 2 in every point $(\mathcal{C}_9, \mathcal{C}_{10})$. We implement every observable analytically with the single exception the $\bar{B} \to X_s\gamma$ branching ratio, for which we use the numerical SM results given in [45]. Contributions to the latter from physics beyond the SM are implemented at leading order. The integrated observables $\langle X \rangle_{q^2_{\min}, q^2_{\max}}$ follow the definition eq. (4.11) with the lower (upper) integration boundary $q^2_{\min}$ $(q^2_{\max})$. In particular we calculate

$$
\chi_{i,\mathrm{E}}\left(\{\mathcal{C}_j\}\right) \equiv
\begin{cases}
\frac{|X_{i,\mathrm{T}} - X_{i,\mathrm{E}}| - \Delta^+_{i,\mathrm{T}}}{\sigma_{i,\mathrm{E}}} & X_{i,\mathrm{E}} \geq X_{i,\mathrm{T}} + \Delta^+_{i,\mathrm{T}} \\
\frac{|X_{i,\mathrm{T}} - X_{i,\mathrm{E}}| - \Delta^-_{i,\mathrm{T}}}{\sigma_{i,\mathrm{E}}} & X_{i,\mathrm{E}} \leq X_{i,\mathrm{T}} - \Delta^-_{i,\mathrm{T}} \\
0 & \text{otherwise}
\end{cases}
\tag{4.20}
$$

with the theoretical prediction of the i-th observable $X_{i,\mathrm{T}} \equiv X_{i,\mathrm{T}}(\{\mathcal{C}_j\})$ and its upper (lower) uncertainty $\Delta^{+(-)}_{i,\mathrm{T}} = \Delta^{+(-)}_{i,\mathrm{T}}(\{\mathcal{C}_j\})$ as described in section 4.1. The experimental result from experiment E for the i-th observable is denoted by $X_{i,\mathrm{E}}$ and its error $\sigma_{i,E}$ is obtained by adding linearly the statistical and systematic errors and subsequent symmetrization. From here we calculate the likelihood $\mathcal{L}$ as

$$
\mathcal{L}(\{\mathcal{C}_j\}) = \exp\left[-\frac{1}{2} \sum_{i,\mathrm{E}} \chi^2_{i,\mathrm{E}}(\{\mathcal{C}_j\})\right].
\tag{4.21}
$$

These scans allow us to constrain the values of the coefficients $\mathcal{C}_9$ and $\mathcal{C}_{10}$ under the assumption that they are real-valued, i.e., there is no CP violation beyond the SM, and that $\mathcal{C}_{1\ldots6,8}$ take on their respective SM values. The $\mathcal{B}(\bar{B} \to X_s\gamma)$ data constrain the magnitude of $\mathcal{C}_7$ strongly to a narrow range of values around $|\mathcal{C}_7^{\mathrm{SM}}|$, however without determining the sign of $\mathcal{C}_7$. For this reason, we present in the following our scans for $\mathcal{C}_7 = \pm\mathcal{C}_7^{\mathrm{SM}}$.

In figure 5 we show the constraints in the $\mathcal{C}_9 - \mathcal{C}_{10}$ plane from $\bar{B} \to \bar{K}^* l^+ l^-$ decays at large recoil and $\bar{B} \to X_s l^+ l^-$ data, without use of the low recoil information. On the other hand, taking into account the $\bar{B} \to \bar{K}^* l^+ l^-$ data at low recoil only, we arrive at the constraints given in figure 6. We see that the latter low recoil constraints are presently much more powerful than the others. An important ingredient for this are the A_{FB} measurements at low recoil constraining $A_{\mathrm{FB}} \propto \mathrm{Re}\{\mathcal{C}_9\mathcal{C}_{10}^*\}$ to be SM-like, the benefits of which have already been pointed out in [17]. The individual constraints, overlaid on top of each other, are given at 68% CL in figure 7. The data are consistent with each other.

The global constraints, obtained after summing over the χ^2-values of all aforementioned data, are shown in figure 8. Two disjoint solutions are favored, around $(\mathcal{C}_9^{\mathrm{SM}}, \mathcal{C}_{10}^{\mathrm{SM}})$ or in the vicinity of $(-\mathcal{C}_9^{\mathrm{SM}}, -\mathcal{C}_{10}^{\mathrm{SM}})$. There appears to be space for order one deviations from either solution, regardless of the sign of $\mathcal{C}_7$. Note that the flipped-sign solution around $(-\mathcal{C}_9^{\mathrm{SM}}, -\mathcal{C}_{10}^{\mathrm{SM}})$ for $\mathcal{C}_7 = \mathcal{C}_7^{\mathrm{SM}}$ is disfavored, see figure 7. Varying $\mathcal{C}_7$ between -0.5 and +0.5 and imposing the $\bar{B} \to X_s\gamma$ constraint leads to barely noticeable larger contours in the $\mathcal{C}_9 - \mathcal{C}_{10}$ plane than the ones in figure 8 a (for $\mathcal{C}_7 < 0$) and figure 8 b (for $\mathcal{C}_7 > 0$), and are not shown.

We find that at 2σ the allowed values of $\mathcal{C}_{10}$ are within $0.5 \leq |\mathcal{C}_{10}| \leq 8$. This gives branching ratios for $\bar{B}_s \to \mu^+\mu^-$ decays enhanced or lowered with respect to the SM one, within the interval $[2 \times 10^{-11}, 1.3 \times 10^{-8}]$. This is consistent with the current upper limit on this mode, $\mathcal{B}(\bar{B}_s \to \mu^+\mu^-) < 3.6 \times 10^{-8}$ (95% CL) [7]. Similarly, the values of the transversity observables $\langle H_T^{(2,3)} \rangle$ integrated over the low recoil region, eq. (4.1), are within the ranges -1.0 and $+0.2$.

As the experimental precision improves over time, especially with the LHCb data at the horizon, there will be opportunities to resolve the 4-fold ambiguity of the current solutions presented in figure 8. Firstly, knowing whether A_{FB} has a zero for low q^2 as in the SM or not, fixes the sign of $\mathrm{Re}\{\mathcal{C}_7\mathcal{C}_{10}^*\}$, thereby eliminating two of the four possible solutions. Alternatively, the sign of the interference term $\mathrm{Re}\{\mathcal{C}_7^*\mathcal{C}_9\}$ in $\mathcal{B}(\bar{B} \to X_s l^+l^-)$ can be extracted from precision measurements. In the SM, this term decreases the branching ratio. These two effects are correlated within our framework, i.e., the existence of an A_{FB} zero crossing implies a destructive interference term in the branching ratio and vice versa.

At this point, there would still be two possible solutions left. Assuming, for instance, a confirmation of the A_{FB} zero, these solutions are $\mathcal{C}_{7,9,10}$ having SM-like signs, or $\mathcal{C}_{7,9,10}$ having opposite signs with respect to their SM values. This last ambiguity can be resolved with precision measurements at the level where one becomes sensitive to the (known) difference between the Wilson coefficients $\mathcal{C}_i$ and the effective ones $\mathcal{C}_i^{\mathrm{eff}}$. Then, the additional contribution breaks the symmetry in the observables under sign reflection. Since the contribution of $\mathcal{C}_7$ to the decay amplitudes is small at large q^2, promising observables to resolve the final sign issue are those at low dilepton masses.

5 Conclusions

Discrepancies between b physics predictions and measurements can be caused by new physics beyond the SM or by an insufficiently accounted for background from strong interaction bound state effects. Due to the decays simple transversality structure at low recoil, these QCD and electroweak effects can be disentangled in $\bar{B} \to \bar{K}^*l^+l^-$ angular studies.

In fact, to leading order in the power corrections with subleading terms being further suppressed, all contributing transversality amplitudes exhibit the same dependence on the short distance electroweak physics, which moreover factorizes from the hadronic matrix elements. This in turn allows to define new observables, $H_T^{(1,2,3)}$, see eqs. (2.13)–(2.15), which do not depend on the form factors at low recoil and cleanly test the SM. Other observables, which do not depend on the Wilson coefficients at low recoil, such as F_{L}, $A_T^{(2,3)}$ and the newly constructed ones in eq. (B.10), probe certain $B \to K^*$ form factors combinations. Measurements of the latter provide input to form factor parametrizations along the lines of [38], which could be compared to (future) lattice results.

Exploiting data we find that the constraints from the low recoil region add significant new information, while being consistent with the large recoil and inclusive decays data, and the SM. Large deviations from the SM are, however, allowed as well due to the current experimental uncertainties. Our findings are summarized in figures 3 and 8. Improved

Observable	SM Prediction	Measurement
$\int_{1.0}^{6.0} \mathrm{d}q^2\mathrm{d}\mathcal{B}(\bar{B}\to X_s l^+l^-)/\mathrm{d}q^2$	$(1.55\pm0.11)\times10^{-6}$ [46, 47]	$\left(1.49^{+0.92}_{-0.83}\right)\times10^{-6}$ [48] $(1.8\pm1.2)\times10^{-6}$ [49]
$\mathcal{B}(\bar{B}\to X_s\gamma)_{E_\gamma>1.6\,\mathrm{GeV}}$	$(3.15\pm0.23)\times10^{-4}$ [45]	$(3.55\pm0.33)\times10^{-4}$ [7]
$\langle\mathcal{B}(\bar{B}\to\bar{K}^*l^+l^-)\rangle_{1.0,6.0}$	$\left(2.60^{+1.82}_{-1.34}\right)\times10^{-7}$ [17]	$\left(1.49^{+0.57}_{-0.52}\right)\times10^{-7}$ [12] $\left(1.60^{+0.68}_{-0.68}\right)\times10^{-7}$ [13]
$\langle A_{\mathrm{FB}}(\bar{B}\to\bar{K}^*l^+l^-)\rangle_{1.0,6.0}$	$+0.05^{+0.04}_{-0.03}$ [17]	$-0.26^{+0.37}_{-0.34}$ [12] $-0.43^{+0.43}_{-0.42}$ [13]
$\langle F_{\mathrm{L}}(\bar{B}\to\bar{K}^*l^+l^-)\rangle_{1.0,6.0}$	$0.73^{+0.13}_{-0.23}$ [17]	$0.67^{+0.28}_{-0.28}$ [12] $0.50^{+0.30}_{-0.33}$ [13]
$\langle\mathcal{B}(\bar{B}\to\bar{K}^*l^+l^-)\rangle_{14.18,16.00}$	$\left(1.32^{+0.43}_{-0.36}\right)\times10^{-7}$ [17]	$\left(1.05^{+0.37}_{-0.34}\right)\times10^{-7}$ [12] $\left(1.51^{+0.49}_{-0.49}\right)\times10^{-7}$ [13]
$\langle A_{\mathrm{FB}}(\bar{B}\to\bar{K}^*l^+l^-)\rangle_{14.18,16.00}$	$-0.44^{+0.07}_{-0.07}$	$-0.70^{+0.32}_{-0.26}$ [12] $-0.42^{+0.25}_{-0.25}$ [13]
$\langle\mathcal{B}(\bar{B}\to\bar{K}^*l^+l^-)\rangle_{16.00,19.21}$	$\left(1.54^{+0.48}_{-0.42}\right)\times10^{-7}$ [17]	$\left(2.04^{+0.43}_{-0.40}\right)\times10^{-7}$ [12] $\left(1.35^{+0.49}_{-0.49}\right)\times10^{-7}$ [13]
$\langle A_{\mathrm{FB}}(\bar{B}\to\bar{K}^*l^+l^-)\rangle_{16.00,19.21}$	$-0.38^{+0.07}_{-0.07}$	$-0.66^{+0.20}_{-0.15}$ [12] $-0.70^{+0.35}_{-0.26}$ [13]

Table 2. The observables used to constrain $\mathcal{C}_{7,9,10}$. The experimental data for A_{FB} have their sign flipped to match the conventions used in this work. For the notation of the observables, see text.

measurements of the forward-backward asymmetry or precision data on the inclusive $\bar{B}\to X_s l^+l^-$ branching ratio can resolve the present ambiguities in the best-fit solution.

Since the decay $\bar{B}_s\to\phi\mu^+\mu^-$ has been seen [13], it becomes relevant in the near future as well. The low recoil framework and our analysis applies to B_s decays with the obvious replacements of masses and hadronic input.

To conclude, we obtained from the existing data on $\bar{B}\to\bar{K}^*l^+l^-$ decays at low recoil new and most powerful constraints. The proposed angular studies offer great opportunities, both in terms of consistency checks and precision, to explore further the borders of the SM.

Acknowledgments

A The angular coefficients

Here, the coefficients $J_i^{(a)}$ in the angular distribution eq. (2.4) are given in terms of the transversity amplitudes $A_{\perp,\|,0,t}$ [24]. Terms with finite lepton masses, which are of relevance

at low q^2, have been kept.

$$J_1^s = \frac{3}{4} \left\{ \frac{(2 + \beta_l^2)}{4} \left[|A_\perp^L|^2 + |A_\parallel^L|^2 + (L \to R) \right] + \frac{4m_l^2}{q^2} \mathrm{Re} \left(A_\perp^L A_\perp^{R*} + A_\parallel^L A_\parallel^{R*} \right) \right\}, \quad \text{(A.1)}$$

$$J_1^c = \frac{3}{4} \left\{ |A_0^L|^2 + |A_0^R|^2 + \frac{4m_l^2}{q^2} \left[|A_t|^2 + 2\mathrm{Re}(A_0^L A_0^{R*}) \right] \right\}, \quad \text{(A.2)}$$

$$J_2^s = \frac{3\beta_l^2}{16} \left[|A_\perp^L|^2 + |A_\parallel^L|^2 + (L \to R) \right], \quad \text{(A.3)}$$

$$J_2^c = -\frac{3\beta_l^2}{4} \left[|A_0^L|^2 + (L \to R) \right], \quad \text{(A.4)}$$

$$J_3 = \frac{3}{8} \beta_l^2 \left[|A_\perp^L|^2 - |A_\parallel^L|^2 + (L \to R) \right], \quad \text{(A.5)}$$

$$J_4 = \frac{3}{4\sqrt{2}} \beta_l^2 \left[\mathrm{Re}(A_0^L A_\parallel^{L*}) + (L \to R) \right], \quad \text{(A.6)}$$

$$J_5 = \frac{3\sqrt{2}}{4} \beta_l \left[\mathrm{Re}(A_0^L A_\perp^{L*}) - (L \to R) \right], \quad \text{(A.7)}$$

$$J_6 = \frac{3}{2} \beta_l \left[\mathrm{Re}(A_\parallel^L A_\perp^{L*}) - (L \to R) \right], \quad \text{(A.8)}$$

$$J_7 = \frac{3\sqrt{2}}{4} \beta_l \left[\mathrm{Im}(A_0^L A_\parallel^{L*}) - (L \to R) \right], \quad \text{(A.9)}$$

$$J_8 = \frac{3}{4\sqrt{2}} \beta_l^2 \left[\mathrm{Im}(A_0^L A_\perp^{L*}) + (L \to R) \right], \quad \text{(A.10)}$$

$$J_9 = \frac{3}{4} \beta_l^2 \left[\mathrm{Im}(A_\parallel^{L*} A_\perp^L) + (L \to R) \right], \quad \text{(A.11)}$$

where

$$\beta_l = \sqrt{1 - \frac{4m_l^2}{q^2}}. \quad \text{(A.12)}$$

The transversity amplitudes at low recoil are given in section 3. The ones at large recoil can be seen in [17].

B   The low recoil transversity observables

It is useful to introduce the (q^2-dependent) quantities

$$U_1 = |A_0^L|^2 + |A_0^R|^2, \quad U_4 = \mathrm{Re}(A_0^L A_\parallel^{L*} + A_0^{R*} A_\parallel^R), \quad U_7 = \mathrm{Im}(A_0^L A_\parallel^{L*} + A_0^{R*} A_\parallel^R), \quad \text{(B.1)}$$

$$U_2 = |A_\perp^L|^2 + |A_\perp^R|^2, \quad U_5 = \mathrm{Re}(A_0^L A_\perp^{L*} - A_0^{R*} A_\perp^R), \quad U_8 = \mathrm{Im}(A_0^L A_\perp^{L*} - A_0^{R*} A_\perp^R), \quad \text{(B.2)}$$

$$U_3 = |A_\parallel^L|^2 + |A_\parallel^R|^2, \quad U_6 = \mathrm{Re}(A_\parallel^L A_\perp^{L*} - A_\parallel^{R*} A_\perp^R), \quad U_9 = \mathrm{Im}(A_\parallel^L A_\perp^{L*} - A_\parallel^{R*} A_\perp^R), \quad \text{(B.3)}$$

which are invariant under the transformations [25]

$$A_i^{L,R} \mapsto e^{i\phi_{L,R}} A_i^{L,R},$$

$$A_{0,\parallel}^{L,R} \mapsto \cos\theta A_{0,\parallel}^{L,R} \mp \sin\theta A_{0,\parallel}^{R,L*}, \qquad A_\perp^{L,R} \mapsto \cos\theta A_\perp^{L,R} \pm \sin\theta A_\perp^{R,L*}. \quad \text{(B.4)}$$

In the limit $m_l \to 0$ the decay rate $\mathrm{d}^4\Gamma$ becomes invariant under the transformations eq. (B.4) as well, reducing the number of 11 independent $J_i^{(a)}$ to 9 [25].

In terms of the J_i, the U_i read

$$U_1 = -\frac{4}{3\beta_l^2} J_2^c, \qquad U_2 = \frac{4}{3\beta_l^2} \left[2J_2^s + J_3\right], \qquad U_3 = \frac{4}{3\beta_l^2} \left[2J_2^s - J_3\right],$$

$$U_4 = \frac{\sqrt{32}}{3\beta_l^2} J_4, \qquad U_5 = \frac{\sqrt{8}}{3\beta_l} J_5, \qquad U_6 = \frac{2}{3\beta_l} J_6, \qquad (\text{B.5})$$

$$U_7 = \frac{\sqrt{8}}{3\beta_l} J_7, \qquad U_8 = \frac{\sqrt{32}}{3\beta_l^2} J_8, \qquad U_9 = -\frac{4}{3\beta_l^2} J_9.$$

Whereas we refer to the $J_i^{(a)}$ as observables which can be extracted from the angular analysis, the U_i greatly simplify the discussion of the form factor related uncertainties.

At high q^2, where we can set m_l to zero safely, the U_i factorize into the short distance $\rho_{1,2}$ and three independent form factor coefficients f_i, $i = 0, \perp, \parallel$ given in section 3.2 as

$$U_1 = 2\rho_1 f_0^2, \qquad U_2 = 2\rho_1 f_\perp^2, \qquad U_3 = 2\rho_1 f_\parallel^2,$$

$$U_4 = 2\rho_1 f_0 f_\parallel, \qquad U_5 = 4\rho_2 f_0 f_\perp, \qquad U_6 = 4\rho_2 f_\parallel f_\perp, \qquad U_7 = U_8 = U_9 = 0. \qquad (\text{B.6})$$

The coefficients J_7, J_8, J_9 and likewise U_7, U_8, U_9 vanish, since they are proportional to $\mathrm{Im}(A_i^X A_j^{X*})$, $i, j = 0, \parallel, \perp$ and by means of the identical short distance dependence of the transversity amplitudes eqs. (3.13)–(3.15).

The simple and factorizable structure of eq. (B.6) allows to test at the same time the SM and the hadronic input used. Firstly, one can construct three independent low recoil transversity observables free of form factors in the HQET symmetry limit, which we define as

$$H_T^{(1)} = \frac{U_4}{\sqrt{U_1 \cdot U_3}}, \qquad (\text{B.7})$$

$$H_T^{(2)} = \frac{U_5}{\sqrt{U_1 \cdot U_2}}, \qquad (\text{B.8})$$

$$H_T^{(3)} = \frac{U_6}{\sqrt{U_2 \cdot U_3}}, \qquad (\text{B.9})$$

see eq. (3.24) and section 2.2 for their explicit expressions in terms of the J_i and the transversity amplitudes. Secondly, ratios of the form factors f_j/f_k can be tested independently of the short distance couplings ρ_i using the observables

$$\frac{f_0}{f_\parallel} = \sqrt{\frac{U_1}{U_3}} = \frac{U_1}{U_4} = \frac{U_4}{U_3} = \frac{U_5}{U_6}, \qquad \frac{f_0}{f_\perp} = \sqrt{\frac{U_1}{U_2}}, \qquad \frac{f_\perp}{f_\parallel} = \sqrt{\frac{U_2}{U_3}} = \frac{\sqrt{U_1 U_2}}{U_4}. \qquad (\text{B.10})$$
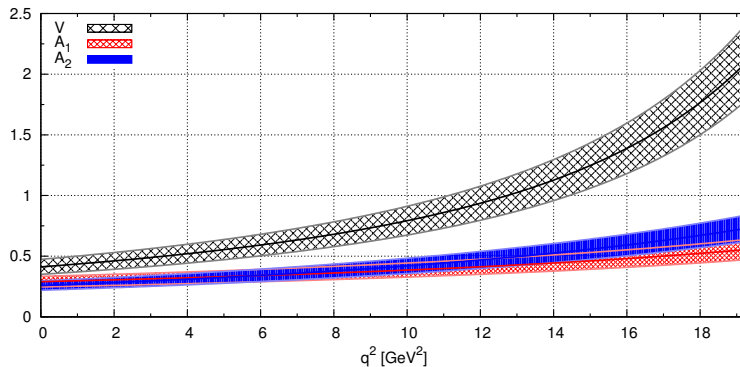
Figure 9. The $B \to K^*$ form factors V, A_1 and A_2 from [37].

C The form factors

The hadronic matrix elements of a B meson with 4-momentum p decaying into a vector meson can be parametrized as [37]:

$$\langle V(k,\epsilon)|\, \bar{q}\gamma_\mu b \,|B(p)\rangle = \frac{2V(q^2)}{m_B+m_V}\varepsilon_{\mu\rho\sigma\tau}\epsilon^{*\rho}p^\sigma k^\tau, \tag{C.1}$$

$$\langle V(k,\epsilon)|\, \bar{q}\gamma_\mu\gamma_5 b \,|B(p)\rangle = i\epsilon^{*\rho}\left[2m_V A_0(q^2)\frac{q_\mu q_\rho}{q^2} + (m_B+m_V)A_1(q^2)\left(g_{\mu\rho}-\frac{q_\mu q_\rho}{q^2}\right)\right.$$
$$\left. -A_2(q^2)\frac{q_\rho}{m_B+m_V}\left((p+k)_\mu - \frac{m_B^2-m_V^2}{q^2}(p-k)_\mu\right)\right], \tag{C.2}$$

$$\langle V(k,\epsilon)|\, \bar{q}i\sigma_{\mu\nu}q^\nu b \,|B(p)\rangle = -2T_1(q^2)\varepsilon_{\mu\rho\sigma\tau}\epsilon^{*\rho}p^\sigma k^\tau, \tag{C.3}$$

$$\langle V(k,\epsilon)|\, \bar{q}i\sigma_{\mu\nu}\gamma_5 q^\nu b \,|B(p)\rangle = iT_2(q^2)\left(\epsilon_\mu^*(m_B^2-m_V^2)-(\epsilon^*\cdot q)(p+k)_\mu\right)$$
$$+ iT_3(q^2)\left(\epsilon^*\cdot q\right)\left(q_\mu - \frac{q^2}{m_B^2-m_V^2}(p+k)_\mu\right), \tag{C.4}$$

where m_V, k and ϵ denote the mass, 4-momentum and the polarization vector of the vector meson, respectively. The seven form factors $V, A_{0,1,2}$ and $T_{1,2,3}$ are functions of the momentum transfer q^2, and $q = p - k$. Note that by parity-invariance $\langle V(k,\epsilon)|\, \bar{q}b \,|B(p)\rangle = 0$.

LCSR provide the form factors at large recoil, $q^2 \lesssim 14\,\text{GeV}^2$ [37]. There, the outcome of the LCSR calculation is fitted to a physical q^2 dependence, of pole or dipole structure. It is conceivable that the form factor parametrization obtained in this way are valid at low recoil as well.

For completeness, we give here the parametrization of the form factors $V, A_{1,2}$ from [37], which we use at both low and large recoil.

$$V(q^2) = \frac{r_1}{1-q^2/m_R^2} + \frac{r_2}{1-q^2/m_{\text{fit}}^2}, \tag{C.5}$$

$$A_1(q^2) = \frac{r_2}{1-q^2/m_{\text{fit}}^2}, \tag{C.6}$$

$$A_2(q^2) = \frac{r_1}{1-q^2/m_{\text{fit}}^2} + \frac{r_2}{(1-q^2/m_{\text{fit}}^2)^2}, \tag{C.7}$$

	r_1	r_2	$m_R^2 \, [\,\mathrm{GeV}^2\,]$	$m_{\mathrm{fit}}^2 \, [\,\mathrm{GeV}^2\,]$
V	0.923	-0.511	5.32^2	49.40
A_1	—	0.290	—	40.38
A_2	-0.084	0.343	—	52.00

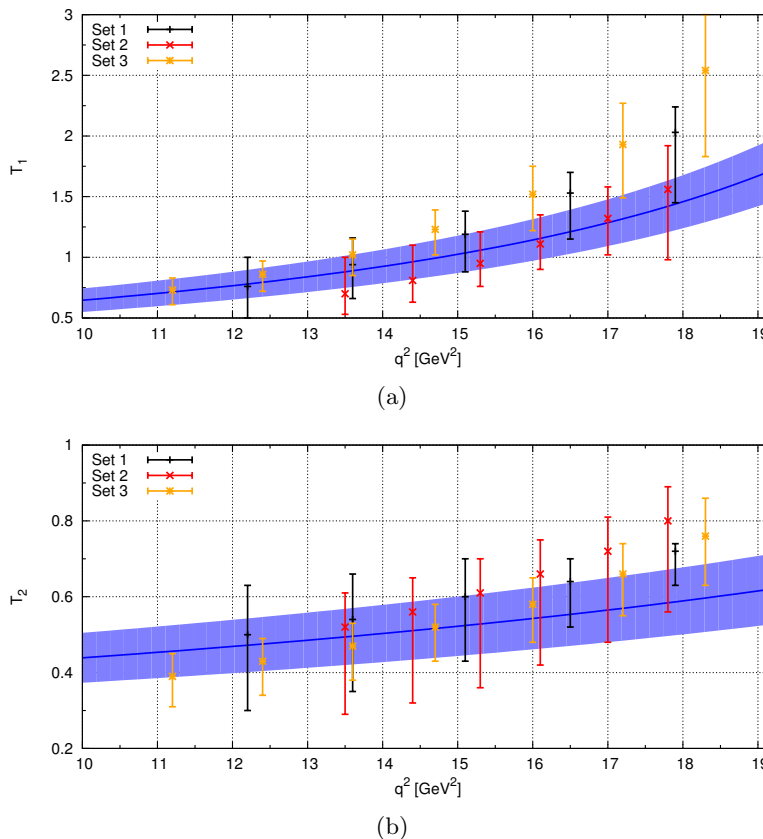**Table 3**. The parameters of the form factors $V, A_{1,2}$.

(a)

(b)

Figure 10. The form factors T_1 (a) and T_2 (b) for $B \to K^*$ transitions from [37] (blue bands) and lattice QCD results (3 data sets) [41].

where the fit parameters $r_{1,2}, m_R^2$ and m_{fit}^2 are given in table 3. The resulting form factors are shown in figure 9. For the uncertainty we use 15 % as follows from the LCSR calculation.

In figure 10 we compare the LCSR fit against the lattice results, which exist for $T_{1,2}$ [41]. The agreement is reasonable, given the substantial uncertainties. There is consistency as well with the preliminary unquenched findings of ref. [42], which are not shown.

How well do the LCSR form factors from [37] satisfy the low recoil form factor relations eq. (3.6)? In figure 11 we show the ratios

$$R_1 = \frac{T_1(q^2)}{V(q^2)}, \qquad R_2 = \frac{T_2(q^2)}{A_1(q^2)}, \qquad R_3 = \frac{q^2}{m_B^2} \frac{T_3(q^2)}{A_2(q^2)}, \qquad \text{(C.8)}$$

which in the symmetry limit should all equal κ, which is also shown. Note, that in the large energy limit $E_{K^*} \gg \Lambda$ the form factors obey to lowest order in the strong coupling very
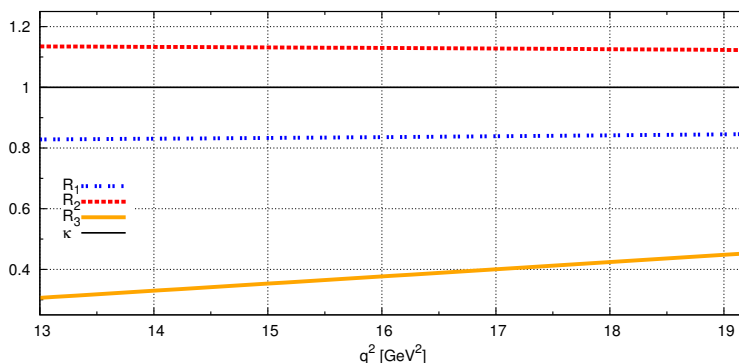
Figure 11. Comparison of the extrapolated LCSR form factors from [37] to the improved Isgur-Wise relations eq. (3.6). Shown is R_1 (blue dotted line), R_2 (red dashed line) and R_3 (golden solid line) as given in eq. (C.8) and $\kappa = 1 + \mathcal{O}(\alpha_s^2)$ for $\mu = m_b(m_b)$ (black thick line).

similar relations $R_{1,2} = 1 + \mathcal{O}(m_{K^*}/m_B)$ and $T_3/A_2 = 1 + \mathcal{O}(m_{K^*}/m_B)$ [34, 50]. We learn that the improved Isgur-Wise relations work reasonably well for the extrapolated LCSR form factors with the exception of the one for T_3. The agreement improves here somewhat if the factor q^2/m_B^2 is replaced by one, its leading term in the heavy quark expansion.

For the low q^2 form factors we employ a factorization scheme within QCDF where the $\xi_{\perp,\parallel}$ are related to the $V, A_{1,2}$ as [15]

$$\xi_\perp = \frac{m_B}{m_B + m_{K^*}} V, \qquad \xi_\parallel = \frac{m_B + m_{K^*}}{2E_{K^*}} A_1 - \frac{m_B - m_{K^*}}{m_B} A_2. \qquad (C.9)$$

Open Access. This article is distributed under the terms of the Creative Commons Attribution Noncommercial License which permits any noncommercial use, distribution, and reproduction in any medium, provided the original author(s) and source are credited.

References

[1] N. Cabibbo, *Unitary symmetry and leptonic decays*, *Phys. Rev. Lett.* **10** (1963) 531 [SPIRES].

[2] M. Kobayashi and T. Maskawa, *CP violation in the renormalizable theory of weak interaction*, *Prog. Theor. Phys.* **49** (1973) 652 [SPIRES].

[3] K. Anikeev et al., *B physics at the Tevatron: run II and beyond*, hep-ph/0201071 [SPIRES].

[4] J.L. Hewett et al., *The discovery potential of a super b factory*, in the proceedings of the *SLAC workshops on flavor physics with a high luminosity asymmetric* e^+e^- *collider*, Stanford, U.S.A. (2003), hep-ph/0503261 [SPIRES].

[5] M. Bona et al., *SuperB: a high-luminosity asymmetric* e^+e^- *super flavor factory. conceptual design report*, arXiv:0709.0451 [SPIRES].

[6] M. Artuso et al., *B, D and K decays*, *Eur. Phys. J.* **C 57** (2008) 309 [arXiv:0801.1833] [SPIRES].

[7] HEAVY FLAVOR AVERAGING GROUP collaboration, E. Barberio et al., *Averages of b-hadron and c-hadron properties at the end of* 2007, see http://www.slac.stanford.edu/xorg/hfag from March 2010, arXiv:0808.1297 [SPIRES].

[8] A. Ali, P. Ball, L.T. Handoko and G. Hiller, *A comparative study of the decays $B \to (K, K^*)$ $\ell^+\ell^-$ in standard model and supersymmetric theories*, *Phys. Rev.* **D 61** (2000) 074024 [hep-ph/9910221] [SPIRES].

[9] F. Krüger, L.M. Sehgal, N. Sinha and R. Sinha, *Angular distribution and CP asymmetries in the decays $\bar{B} \to K^-\pi^+e^-e^+$ and $\bar{B} \to \pi^-\pi^+e^-e^+$*, *Phys. Rev.* **D 61** (2000) 114028 [*Erratum ibid.* **D 63** (2001) 019901] [hep-ph/9907386] [SPIRES].

[10] BABAR collaboration, B. Aubert et al., *Measurements of branching fractions, rate asymmetries and angular distributions in the rare decays $B \to K\ell^+\ell^-$ and $B \to K^*\ell^+\ell^-$*, *Phys. Rev.* **D 73** (2006) 092001 [hep-ex/0604007] [SPIRES].

[11] BABAR collaboration, B. Aubert et al., *Angular distributions in the decays $B \to K^*\ell^+\ell^-$*, *Phys. Rev.* **D 79** (2009) 031102 [arXiv:0804.4412] [SPIRES].

[12] BELLE collaboration, J.T. Wei et al., *Measurement of the differential branching fraction and forward-backword asymmetry for $B- > K^*\ell^+\ell^-$*, *Phys. Rev. Lett.* **103** (2009) 171801 [arXiv:0904.0770] [SPIRES].

[13] H. Miyake et al., *Measurement of forward-backward asymmetry in $B \to K^{(*)}\mu^+\mu^-$ and first observation of $B_s^0 \to \phi\mu^+\mu^-$*, CDF Public note 10047.

[14] M. Beneke, T. Feldmann and D. Seidel, *Systematic approach to exclusive $B \to V \ell^+\ell^-$, $V\gamma$ decays*, *Nucl. Phys.* **B 612** (2001) 25 [hep-ph/0106067] [SPIRES].

[15] M. Beneke, T. Feldmann and D. Seidel, *Exclusive radiative and electroweak $b \to d$ and $b \to s$ penguin decays at NLO*, *Eur. Phys. J.* **C 41** (2005) 173 [hep-ph/0412400] [SPIRES].

[16] B. Grinstein and D. Pirjol, *Precise $|V_{ub}|$ determination from exclusive B decays: controlling the long-distance effects*, *Phys. Rev.* **D 70** (2004) 114005 [hep-ph/0404250] [SPIRES].

[17] C. Bobeth, G. Hiller and G. Piranishvili, *CP asymmetries in bar $B \to \bar{K}^*(\to \bar{K}\pi)\ell\ell$ and untagged $\bar{B}_s$, $B_s \to \phi(\to K^+K^-)\ell\ell$ decays at NLO*, *JHEP* **07** (2008) 106 [arXiv:0805.2525] [SPIRES].

[18] T. Hurth and D. Wyler, in J.L. Hewett et al. [4].

[19] B. Grinstein and D. Pirjol, *Symmetry-breaking corrections to heavy meson form-factor relations*, *Phys. Lett.* **B 533** (2002) 8 [hep-ph/0201298] [SPIRES].

[20] N. Isgur and M.B. Wise, *Relationship between form-factors in semileptonic anti-B and D decays and exclusive rare anti-B meson decays*, *Phys. Rev.* **D 42** (1990) 2388 [SPIRES].

[21] F. Krüger and L.M. Sehgal, *Lepton polarization in the decays $B \to X_s\mu^+\mu^-$ and $B \to X_s\tau^+\tau^-$*, *Phys. Lett.* **B 380** (1996) 199 [hep-ph/9603237] [SPIRES].

[22] K.G. Chetyrkin, M. Misiak and M. Münz, *Weak radiative B-meson decay beyond leading logarithms*, *Phys. Lett.* **B 400** (1997) 206 [*Erratum ibid.* **B 425** (1998) 414] [hep-ph/9612313] [SPIRES].

[23] C. Bobeth, G. Hiller and G. Piranishvili, *Angular distributions of $B \to Kll$ decays*, *JHEP* **12** (2007) 040 [arXiv:0709.4174] [SPIRES].

[24] F. Krüger and J. Matias, *Probing new physics via the transverse amplitudes of $B_0 \to K_0^*$ $(\to K^-\pi^+) \ell^+\ell^-$ at large recoil*, *Phys. Rev.* **D 71** (2005) 094009 [hep-ph/0502060] [SPIRES].

[25] U. Egede, T. Hurth, J. Matias, M. Ramon and W. Reece, *New observables in the decay mode $\bar{B} \to \bar{K}_0^* \ell^+\ell^-$*, *JHEP* **11** (2008) 032 [arXiv:0807.2589] [SPIRES].

[26] W. Altmannshofer et al., *Symmetries and asymmetries of $B \to K^* \mu^+ \mu^-$ decays in the standard model and beyond*, *JHEP* **01** (2009) 019 [arXiv:0811.1214] [SPIRES].

[27] U. Egede, T. Hurth, J. Matias, M. Ramon and W. Reece, *New physics reach of the decay mode $\bar{B} \to \bar{K}^{*0} \ell^+ \ell^-$*, arXiv:1005.0571 [SPIRES].

[28] A. Bharucha and W. Reece, *Constraining new physics with $B \to K^* \mu^+ \mu^-$ in the early LHC era*, arXiv:1002.4310 [SPIRES].

[29] A.V. Manohar and M.B. Wise, *Heavy quark physics*, *Camb. Monogr. Part. Phys. Nucl. Phys. Cosmol.* **10** (2000) 1 [SPIRES].

[30] D. Seidel, *Analytic two-loop virtual corrections to $b \to d \ell^+ \ell^-$*, *Phys. Rev.* **D 70** (2004) 094038 [hep-ph/0403185] [SPIRES].

[31] H.H. Asatrian, H.M. Asatrian, C. Greub and M. Walker, *Two-loop virtual corrections to $B \to X_s \ell^+ \ell^-$ in the standard model*, *Phys. Lett.* **B 507** (2001) 162 [hep-ph/0103087] [SPIRES].

[32] H.M. Asatrian, K. Bieri, C. Greub and M. Walker, *Virtual- and Bremsstrahlung corrections to $b \to d \ell^+ \ell^-$ in the standard model*, *Phys. Rev.* **D 69** (2004) 074007 [hep-ph/0312063] [SPIRES].

[33] B. Grinstein and D. Pirjol, *Subleading corrections to the $|V_{ub}|$ determination from exclusive B decays*, *Phys. Lett.* **B 549** (2002) 314 [hep-ph/0209211] [SPIRES].

[34] G. Burdman and G. Hiller, *Semileptonic form-factors from $B \to K^* \gamma$ decays in the large energy limit*, *Phys. Rev.* **D 63** (2001) 113008 [hep-ph/0011266] [SPIRES].

[35] PARTICLE DATA GROUP collaboration, C. Amsler et al., *Review of particle physics*, *Phys. Lett.* **B 667** (2008) 1 [SPIRES].

[36] TEVATRON ELECTROWEAK WORKING GROUP collaboration, *Combination of CDF and D0 results on the mass of the top quark*, arXiv:0903.2503 [SPIRES].

[37] P. Ball and R. Zwicky, *$B_{d,s} \to \rho, \omega, K^*, \phi$ decay form factors from light-cone sum rules revisited*, *Phys. Rev.* **D 71** (2005) 014029 [hep-ph/0412079] [SPIRES].

[38] A. Bharucha, T. Feldmann and M. Wick, *Theoretical and phenomenological constraints on form factors for radiative and semi-leptonic B-meson decays*, arXiv:1004.3249 [SPIRES].

[39] SPQCDR collaboration, A. Abada et al., *Heavy to light vector meson semileptonic decays*, *Nucl. Phys. Proc. Suppl.* **119** (2003) 625 [hep-lat/0209116] [SPIRES].

[40] J.M. Flynn, Y. Nakagawa, J. Nieves and H. Toki, *$|V_{ub}|$ from exclusive semileptonic $B \to \rho$ decays*, arXiv:0812.2795 [SPIRES].

[41] D. Becirevic, V. Lubicz and F. Mescia, *An estimate of the $B \to K^* \gamma$ form factor*, *Nucl. Phys.* **B 769** (2007) 31 [hep-ph/0611295] [SPIRES].

[42] Z. Liu et al., *Form factors for rare B decays: strategy, methodology and numerical study*, arXiv:0911.2370 [SPIRES].

[43] M. Bauer, S. Casagrande, U. Haisch and M. Neubert, *Flavor physics in the Randall-Sundrum Model: II. Tree-level weak-interaction processes*, arXiv:0912.1625 [SPIRES].

[44] THE LHCB collaboration, et al., *Roadmap for selected key measurements of LHCb*, arXiv:0912.4179 [SPIRES].

[45] M. Misiak et al., *The first estimate of $B(\bar{B} \to X_s \gamma)$ at $O(\alpha_s^2)$*, *Phys. Rev. Lett.* **98** (2007) 022002 [hep-ph/0609232] [SPIRES].

[46] C. Bobeth, P. Gambino, M. Gorbahn and U. Haisch, *Complete NNLO QCD analysis of* $\bar{B} \to X_s\ \ell^+\ell^-$ *and higher order electroweak effects*, *JHEP* **04** (2004) 071 [hep-ph/0312090] [SPIRES].

[47] T. Huber, E. Lunghi, M. Misiak and D. Wyler, *Electromagnetic logarithms in* $\bar{B} \to X_s\ \ell^+\ell^-$, *Nucl. Phys.* **B 740** (2006) 105 [hep-ph/0512066] [SPIRES].

[48] BELLE collaboration, M. Iwasaki et al., *Improved measurement of the electroweak Penguin process* $B \to X_s\ \ell^+\ell^-$, *Phys. Rev.* **D 72** (2005) 092005 [hep-ex/0503044] [SPIRES].

[49] BABAR collaboration, B. Aubert et al., *Measurement of the* $B \to X_s\ell^+\ell^-$ *branching fraction with a sum over exclusive modes*, *Phys. Rev. Lett.* **93** (2004) 081802 [hep-ex/0404006] [SPIRES].

[50] J. Charles, A. Le Yaouanc, L. Oliver, O. Pene and J.C. Raynal, *Heavy-to-light form factors in the heavy mass to large energy limit of QCD*, *Phys. Rev.* **D 60** (1999) 014001 [hep-ph/9812358] [SPIRES].